Transduction of inflammation from peripheral immune cells to the hippocampus induces neuronal hyperexcitability mediated by Caspase-1 activation

Tarek Shaker (tarek.shaker@umontreal.ca)
Universite de Montreal - Centre de recherche du CHU Sainte Justine https://orcid.org/0000-0001-8329-4101

Bidisha Chattopadhyaya
CHU Sainte-Justine Centre de Recherche: Centre Hospitalier Universitaire Sainte-Justine Centre de Recherche

Bénédicte Amilhon
Université de Montréal: Universite de Montreal

Graziella Di Cristo
Université de Montréal: Universite de Montreal

Alexander G. Weil
Université de Montréal: Universite de Montreal

Research

Keywords: Caspase-1, hippocampus, hyperexcitability, inflammasome, organotypic cultures, peripheral blood mononuclear cells

Posted Date: November 23rd, 2020

DOI: https://doi.org/10.21203/rs.3.rs-111417/v1

Version of Record: A version of this preprint was published at Neurobiology of Disease on December 1st, 2021. See the published version at https://doi.org/10.1016/j.nbd.2021.105535.

Abstract

1.1. Background Recent studies report infiltration of peripheral blood mononuclear cells (PBMCs) into the central nervous system (CNS) in epileptic disorders, suggestive of a potential contribution of PBMC extravasation to the generation of seizures. Nevertheless, the underlying mechanisms involved in PBMC infiltrates promoting neuronal predisposition to ictogenesis remain unclear. Therefore, we developed an *in vitro* model mimicking infiltration of activated PBMCs into the brain in order to investigate potential transduction of inflammatory signals from PBMCs to the CNS.

1.2. Methods To establish our model, we first extracted PBMCs from rat spleen, then, immunologically primed PBMCs with lipopolysaccharide (LPS), followed by further activation with nigericin. Thereafter, we co-cultured these activated PBMCs with organotypic cortico-hippocampal brain slice cultures (OCHSCs) derived from the same rat, and compared PBMC-OCHSC co-cultures to OCHSCs exposed to PBMCs in the culture media. We further targeted a potential molecular pathway underlying transduction of peripheral inflammation to OCHSCs by incubating OCHSCs with the Caspase-1 inhibitor VX-765 prior to co-culturing PBMCs with OCHSCs. After 24 hours, we analyzed inflammation markers in the cortex and the hippocampus using semiquantitative immunofluorescence. In addition, we analyzed neuronal activity by whole-cell patch-clamp recordings in cortical layer II/III and hippocampal CA1 pyramidal neurons.

1.3. Results In the cortex, co-culturing immunoreactive PBMCs treated with LPS + nigericin on top of OCHSCs upregulated inflammatory markers and enhanced neuronal excitation. In contrast, no excitability changes were detected after adding primed PBMCs (i.e. treated with LPS only), to OCHSCs. Strikingly, in the hippocampus, both immunoreactive and primed PBMCs elicited similar pro-inflammatory and pro-excitatory effects. However, when immunoreactive and primed PBMCs were cultured in the media separately from OCHSCs, only immunoreactive PBMCs gave rise to neuroinflammation and hyperexcitability in the hippocampus, whereas primed PBMCs failed to produce any significant changes. Finally, VX-765 application to OCHSCs, co-cultured with either immunoreactive or primed PBMCs, protected them from neuroinflammation and hippocampal hyperexcitability.

1.4. Conclusions Our study shows a higher susceptibility of the hippocampus to peripheral inflammation as compared to the cortex, mediated via Caspase-1-dependent signaling pathways. Thus, our findings suggest that Caspase-1 inhibition may potentially provide therapeutic benefits during hippocampal neuroinflammation and hyperexcitability secondary to peripheral innate immunity.

2. Introduction

Systemic inflammation has been linked to the subsequent development of epileptic disorders, such as febrile infection-related epilepsy syndrome (1), temporal lobe epilepsy associated with prolonged febrile seizures (2) and Rasmussen encephalitis (3). Nevertheless, how systemic inflammation contributes to the pathogenesis of epileptic seizures is not known yet. Recent evidence suggests that penetration of peripheral immune cells, namely peripheral blood mononuclear cells (PBMCs), into the central nervous

system (CNS) following peripheral inflammation may potentially render the brain vulnerable to epileptogenesis. Indeed, experimental epilepsy models indicate that the presence of PBMC infiltrates in the brain promotes seizure development (4, 5). On the other hand, evoking peripheral inflammation in experimental animals has revealed that cellular and molecular mechanisms besides PBMCs recruitment to the brain also contribute to inflammation-induced facilitation of epileptiform activity (6). Such inflammatory processes include pro-inflammatory cytokines infiltrating the blood-brain barrier and increasing neuronal excitability via binding to cognate receptors on neuronal, glial and perivascular cells (7). Moreover, reactive microglia can produce cytokines as a secondary "mirror" response to peripheral inflammation, hence, activating localized neuroinflammation in the CNS despite the lack of peripheral cell infiltrates (reviewed in 6). Therefore, the role of PBMC extravasation on seizure precipitation is still not clear.

Induction of peripheral immunity in experimental models has typically focused on activating pattern-recognition receptors, namely Toll-like receptors (TLRs) and NOD-like receptor (NLRs) (8). While TLRs are localized to either the cellular or endosomal membranes, and sense mainly pathogen-associated molecular patterns, such as bacterial cell wall components and viral RNA (8), NLRs are found in the cytosol (8) and predominantly sense intracellular stressors, such as ion flux or reactive oxygen species (9, 10). The sequential engagement of TLR4 (Signal 1) and NLRP3 (Signal 2) has been shown to trigger the activation of the inflammasome, a cytosolic multiprotein signalling complex that facilitates the activation of Caspase-1 family proteases (11, 12). Caspase-1 activation mediates the maturation and secretion of pro-inflammatory cytokines like interleukin (IL)-1β and IL-18 (12, 13). In this two-signal system, the initial priming step (signal 1) requires TLR4 binding to a cognate ligand, e.g. the gram-negative bacterial-derived cell-wall component lipopolysaccharide (LPS) (14). This triggers the downstream nuclear factor κB pathway leading to the transcriptional and/or translational upregulation of inflammasome components and substrates, including the precursor form of IL-1β (pro-IL-1β) (12). In response to a subsequent signal (or signal 2), such as nigericin,, a drop in intracellular K^+ concentration stimulates NLRP3 to recruit apoptosis-associated speck-like protein containing a carboxy-terminal CARD (ASC) adaptor protein and the interleukin-1 converting enzyme Caspase-1, which is normally expressed in its inactive form, i.e. pro-Caspase-1 (12, 14). Assembly of the NLRP3-ASC-Caspase-1 inflammasome complex (also known as the NLRP3 inflammasome) catalyzes the proteolytic conversion of pro-Caspase-1 to active Caspase-1. Activation of Caspase-1 subsequently promotes the proteolytic maturation and release of IL-1β and IL-18 (12). Of interest, *in vivo* systemic administration of LPS produced a lower seizure threshold and an increase of neuronal excitability (7), suggesting that peripheral stimulation of TLR4 modulates seizure activity. Also, recent clinical studies posited that seizure propensity was directly proportional to peripheral expression of NLRP3 and IL-1β (15, 16). Nevertheless, to date, the fundamental underpinnings by which peripheral activation of the TLR4-NLRP3 two-signal pathway enhance seizure susceptibility are unknown, and the role of penetrating pro-inflammatory PBMCs through the blood-brain barrier remains to be determined.

Several *in vivo* studies of young rodents indicate that the hippocampus is particularly vulnerable to peripheral immune challenges that activate TLR4 pathway, including heightened seizure susceptibility and memory-related deficits (7, 17–19). Such challenges were found to trigger pathological ramifications at the molecular level that resulted in excitation/inhibition imbalance in the hippocampus, e.g. increased expression of glutamate receptors and a shift of GABA-mediated currents from hyperpolarizing to depolarizing values (20, 21). Together, these results suggest that systemic inflammation produces neuropathological changes in the hippocampus through alteration of intrinsic neuronal properties. *In vitro* cultures of brain-derived cells can complement *in vivo* experimental models by providing a simple and accessible approach to unmask potential contribution of different cellular and molecular players involved in transduction of peripheral inflammation to the hippocampus. In contrast to classical *in vitro* preparations, organotypic slice cultures preserve the organization of different cell types along with the cytoarchitecture and neural circuitry of the original tissue, hence ensuring high resemblance of the cultured tissue to their counterparts *in vivo* (22). Additionally, the physiological and morphological characteristics of different types of neurons frequently match those of neurons studied in acute brain slices (22–24). Therefore, we sought to use organotypic slice cultures to investigate the cellular and molecular mechanisms responsible for PBMC-mediated inflammatory processes in the hippocampus.

To test the hypothesis that PBMC extravasation following peripheral induction of NLRP3 inflammasomes could elicit pathophysiological changes in brain excitability, we developed a novel *in vitro* co-culture model to reproduce the interaction of pro-inflammatory PBMCs with CNS tissue. The model consists of activating inflammasomes in spleen-derived PBMCs, and culturing these cells alongside organotypic brain slices containing the hippocampus and overlying cortex, i.e. organotypic cortico-hippocampal brain slice cultures (OCHSCs). We found that adding pro-inflammatory PBMCs to naive OCHSCs gave rise to inflammasome formation and enhanced neuronal excitability in both cortical and hippocampal tissue. Moreover, we revealed that PBMC-induced pro-excitatory effects in OCHSC neurons were mediated by occlusion of the 4-aminopyridine (4-AP) sensitive K^+ currents: A-type fast activating, fast inactivating current (I_A) and D-type fast activating, slowly inactivating current (I_D). Finally, by selectively targeting Caspase-1 catalytic activation, we demonstrated that inflammation transduction between PBMCs and the CNS is regulated by Caspase-1 activation.

3. Materials And Methods

3.1. Experimental animals

Sprague–Dawley rats purchased from Charles River Laboratories (St. Constant, Quebec, Canada) were used in all experiments. Measures were taken to minimize the number of animals used.

3.2. OCHSC preparation

Brain tissue was obtained from male rat pups at postnatal days 9 and 10 (P9/P10). Animals were decapitated, and the brain was immediately removed and immersed in ice-cold modified Hanks' Balanced Salt Solution (HBSS) optimized for slice preparation (slicing solution): GIBCO HBSS containing calcium

(Ca^{2+}) and magnesium (Mg^{2+}) (ThermoFisher Sciences), supplemented with 30 mM glucose, and 0.5 mM kynurenic acid; the pH was adjusted to 7.3–7.4, and osmolarity to 310–315 mOsm/L. Under sterile conditions, brains were hemisected and submerged in liquid agarose: low melting point TopVision agarose (ThermoFisher Sciences) dissolved in slicing solution (2% weight/volume) pre-warmed at 37ºC. Once solidified, the brain-containing agarose block was mounted on a slicing stage with superglue and ~ 350 µm coronal slices of the dorsal frontal brain were cut with a vibrating blade microtome VT-1000-S (Leica Microsystems). Slices that contained the dorsal hippocampus and the overlying cortex were collected and transferred to a Petri dish containing slicing solution and incubated at 4ºC for 1-1.5 hours. Individual slices were placed on 12 mm porous (0.4 µm) Millicell membrane inserts (Millipore-Sigma) at an interface with culture medium (one slice per insert) in 24-well culture plates, and put inside a 5% CO_2 incubator at 34ºC. After 48 hours, OCHSCs were incubated with a cocktail of anti-mitotic drugs diluted in OCHSC culture medium to inhibit glial proliferation, which throughout the course of our experiments resulted in the majority of OCHSCs returning to a resting ramified state by 4–5 days in vitro (DIV). The cocktail consisted of the following (in µg/mL): 1.5 cytosine-β-D-arabino-funanoside (Millipore-Sigma), 1.5 uridine (Millipore-Sigma), and 1.55-Fluro-2'-deoxyuridine (Millipore-Sigma). Fresh medium was added after 24 hours, and afterwards the medium was changed every 2 days till the end of the experiment. The composition of OCHSC culture medium was the following: 50% minimum essential medium (with 25 mM HEPES), 20% heat inactivated horse serum, 25% HBSS containing Ca^{2+} and Mg^{2+}, 1 mM GlutaMAX, 0.5 mM L-ascorbic acid, 55 mM glucose, 50–100 U/mL Penicillin-Streptomycin; pH 7.3–7.4; 310–315 mOsm/L. All components of the culture medium were supplied by ThermoFisher Sciences.

3.3. PBMC isolation and culturing

In parallel with brain tissue extraction, the spleen was quickly harvested from the same animal and kept in cold phosphate buffered saline (PBS), pH 7.4. Under a laminar flow hood, the spleen was homogenized and placed on top of a 70 µm Falcon cell strainer (ThermoFisher Sciences). Splenocytes were washed through the strainer with cold PBS, and cells were centrifuged. Splenocytes were thereafter centrifuged at 300 × *g* for 5 min at room temperature throughout all experimental protocols. Cell pellet was resuspended in ACK lysing buffer and incubated for 5 min to osmotically lyse erythrocytes before adding 10 × volume of PBS to relieve the osmotic pressure. Subsequently, spleen-derived PBMCs were centrifuged, resuspended in culture medium at a confluency of 1-1.5 × 10^6 cells/mL in a T25 flask, and transferred to a 5% CO_2 incubator at 37ºC. At 3 DIV, PBMCs were passaged by aspirating the medium-suspended portion of cells, mainly lymphocytes, whereas adherent cells, mainly monocytes, were detached using 0.05% trypsin. After combining all PBMC cell types, cells were centrifuged, washed with PBS, and centrifuged again before being resuspended in PBMC culture medium at a confluency of 1-1.5 × 10^6 cells/mL, and then transferred to a 5% CO_2 incubator at 37ºC. The composition of PBMC culture medium was the following: 80% high glucose Dulbecco's modified eagle medium, 10% fetal bovine serum, 1% non-essential amino-acids, 1 mM sodium pyruvate, 2 mM L-glutamine, 50 µM β-mercaptophenol, 50–100 U/mL Penicillin-Streptomycin; pH 7.3–7.4.All reagents were obtained from ThermoFisher Sciences.

3.4 PBMC activation and co-culturing with OCHSCs

In the established protocol of TLR4-NLRP3 two-signal pathway activation (9, 12, 14), TL4 stimulation (signal 1) is conditional for prompting NLRP3 inflammasome oligomerization (signal 2).Therefore, both signals 1 and 2 were sequentially induced at 6 DIV by first adding the TL4 ligand LPS (*Escherichia* coli serotype 0111: B4; Millipore-Sigma) at a concentration of 1 µg/ml to PBMCs, and 3-3.5 hours later, 10 µM of the K^+ ionophore nigericin (InvivoGen) was added to the LPS-treated PBMCs for 2.5-3 hours. In some cultures, PBMCs were incubated only with LPS for 3-3.5 hours without adding nigericin, i.e. LPS-primed PBMCs (signal 1 only), and the rest of PBMCs were left untreated (naive PBMCs). Afterwards, LPS and nigericin were washed out by centrifugation, followed by resuspending the cell pellet in PBS, and washing all PBMC groups in OCHSC culture medium twice. Finally, PBMCs were collected by centrifugation. The PBMC-OCHSC co-culture system was established by seeding PBMCs on top of layer I of the cortex of OCHSCs at a concentration of ~ 3.0×10^4 cells per OCHSC. For PBMC media incubation, ~ 9.0×10^4 cells were added to the media of OCHSCs.

3.5. VX-765 Treatment

On 6 DIV, one hour prior to co-culturing PBMCs with OCHSCs, regular OCHSC medium was replaced with serum-free medium, which contains all components of the regular medium except for heat inactivated horse serum. The selective Caspase-1 inhibitor, VX-765 (or Belnacasan, MedChemExpress, stock concentration 196.4 mM dissolved in DMSO) was added to serum-free medium at a final concentration of 100 µM, and 0.055% final DMSO volume. Concentration of VX-765 was selected based on an earlier study, which optimized the VX-765 dosage needed to inhibit NLRP3 inflammasome activation in organotypic hippocampal slice cultures (25). For control experiments, only the vehicle, i.e. DMSO, was added to the medium at the same volume. PBMC-OCHSC co-cultures were incubated with VX-765 overnight, and utilized for electrophysiology and immunohistochemistry experiments the next day, i.e. 7 DIV.

3.6. PBMC labeling with cell-tracing dye

For immunostaining experiments analyzing PBMC migration across OCHSCs, PBMCs were fluorescently labeled with the long-term cytoplasmic dye carboxyfluorescein diacetate succinimidyl ester (CFSE) as per the company's protocol (ThermoFisher Sciences) with some modifications (see below). At 6DIV, PBMCs were aspirated and trypsinized as in the PBMC passaging protocol (see Sect. 2.3. PBMC isolation and culturing). After combining all PBMC cell types, cells were centrifuged, washed with PBS, and centrifuged again. Then, the supernatant was discarded and cell pellet was resuspended in pre-warmed (37ºC) PBS. CellTrace far red CFSE dye (ThermoFisher Sciences) was added to PBMCs (1:5,000 dilution), and cells were incubated with the dye at 37ºC for 20 min. Afterwards, cells were centrifuged, and the pellet was washed with cold PBMC culture medium to washout unbound dye, followed by centrifugation. The pellet was resuspended in warm PBMC culture medium (with 20% fetal bovine serum), and cells were incubated at 37ºC for 5–10 min to quench remaining excess dye. Finally, cells were washed with OCHSC culture medium, the pellet was collected by centrifugation, and PBMCs were seeded either on top of OCHSCs or into OCHSC medium as above. After 2 hours, OCHSCs were fixed for 2 hours at 4 °C in 4%

paraformaldehyde in PBS, pH 7.4, washed three times with PBS for 10 minutes, and mounted with Vectashield (Vector Labs). No antibodies were used for imaging of fluorescent $CFSE^+$ PBMCs.

3.7. Immunohistochemistry

All OCHSCs used for immunohistochemistry were collected at 7 DIV. In brief, OCHSCs were fixed for 2 hours at 4 °C in 4% paraformaldehyde in PBS, pH 7.4, washed three times with PBS for 10 minutes, then cryoprotected in 30% sucrose solution in PBS. OCHSCs were blocked in 10% normal goat serum and 1% Triton X-100 in 1 × TBS (50 mM Tris–HCl, 150 mM NaCl, pH 7.4) for 2 hours at room temperature, and then incubated overnight at 4 °C in 10% normal goat serum, 0.3% Triton X-100 and primary antibodies diluted in 1 × TBS. Next, OCHSCs were washed three times in 1 × TBST (0.3% Triton X-100 in 1 × TBS) for 10 minutes, then incubated with secondary antibodies diluted in 1 × TBST for 2 hours at room temperature, before washing the OCHSCs again three times with 1 × TBST for 10 minutes. Finally, 4',6-diamidino-2-phenylindole (DAPI) (Millipore-Sigma) diluted in 1 × TBST (1/10,000) was applied for 5 minutes, then the OCHSCs were washed three times in 1 × TBST for 10 minutes and mounted with Vectashield (Vector Labs). The following primary antibodies were used: mouse anti-ASC (1:250; Cat. No. sc-514414, Santa Cruz), mouse anti-NeuN (1:250; Cat. No. MAB377, Millipore-Sigma), rabbit anti-NLRP1 (1:1,000; Cat. No. 4990, Cell Signaling), rabbit anti-NLRP3 (1:500; Cat. No. LS-C334192, LifeSpan Biosciences). In addition, the following secondary antibodies were used: Alexa 488- and 594-conjugated goat IgG (1: 1,000; Molecular Probes). Specific quantification values for immunohistochemistry data are reported in Table S1 [see Additional file 1].

3.8. Confocal microscopy

All imaging was performed on Leica Confocal microscope (LEICA TCS SP8) equipped with a motorized x–y–z stage control. Non-overlapping images from a single confocal plane were acquired with 20x (NA 0.75) and oil-immersion 63x (NA 1.40) objectives. Image acquisition settings were the following: pinhole 1 airy unit, scan speed 400 Hz unidirectional, format 1024 × 1024, z-step as indicated by the software for each objective. The appropriate excitation wavelengths for blue (DAPI), green (Alexa-Fluor 488) and red (Alexa-Fluor 594) channels were used in a sequential order to eliminate any potential cross-talk, especially when imaging two or more channels. Images for individual antibodies (for example Nlrp1, Nlrp3 and ASC) were acquired using the same acquisition parameters. Bright-field images were taken in transmitted brightfield illumination. Since microglia close to the surface of OCHSCs can remain in the activated state up to 6 DIV (26), we excluded the upper 50 µm of OCHSC tissue, and we imaged only the central zone along the z-axis of OCHSCs to produce composite images.

3.9. Electrophysiology

Patch-clamp electrophysiological recordings in the whole-cell configuration were conducted between 7–11 DIV. On the day of the recording, individual OCHSCs were removed from the incubator, placed into a recording chamber, and continuously perfused with a pre-warmed (33 ± 1ºC) carbogenated artificial cerebrospinal fluid (ACSF) at a rate of 2–3 mL/min, which contained the following (in mM): 124 NaCl, 3 KCl, 1.3 $MgSO_4$-H_2O, 1.4 NaH_2PO_4, 10 D-glucose, 26 $NaHCO_3$ and 2.5 $CaCl_2$ (pH 7.3–7.4; 320–325 mOsm/L). Based on cell morphology and the presence of a large apical dendrite, layer II/III cortical

and CA1 hippocampal pyramidal cells were visually identified with an upright microscope (Olympus) attached to a differential interference contrast optics and infrared video camera (Hitachi Kokusai Electric). Recording pipettes were pulled from borosilicate glass (World Precision Instruments) with a PP-83 two-stage puller (Narishige) to a resistance range of 5–7 MΩ when backfilled with intracellular solution containing (in mM): 129 K-gluconate, 10 HEPES, 5 KCl, 5 MgATP, 0.3 NaGTP, 1 EGTA and 0.3 $CaCl_2$. The pH and osmolarity were adjusted to 7.20–7.25 with KOH, and 300–305 mOsm/L, respectively. Biocytine (0.05–0.1%) was added to the intracellular solution for post-hoc confirmation of cell identity. Upon formation of a tight seal (> 1 GΩ) on pyramidal cell bodies, whole-cell configuration was achieved by rupturing the membrane with negative pressure. Cell recordings were amplified and low-pass filtered at 1 kHz using Axopatch 200B amplifier (Molecular Devices), digitized with a Digidata 1440A analog-digital converter (Molecular Devices), and signals were acquired at a sampling rate of 10 kHz using the pCLAMP software 10.4 (Molecular Devices).

Once the whole-cell configuration was established, neurons were held at -60 mV for 4–6 minutes in voltage-clamp before experimental recordings. Neurons were only included in the analysis if they have shown stable (< 15%) holding current and access resistance in voltage-clamp throughout recording. Neuronal resting membrane potential was measured by averaging the potential over a 1 min period of passive recording in current-clamp. Rheobase, which is the minimum current required to elicit an action potential, was measured in current clamp with no holding current applied by injecting successive sweeps of incremental depolarizing current ramps at 100 pA per sweep. Repolarization time was measured as the outward current during the repolarization phase of the action potential, i.e. between the peak of the action potential and the trough after the action potential.

To determine the amplitude of 4-AP sensitive K^+ currents I_A and I_D, cell output was measured in response to incremental successive voltage steps in the voltage-clamp configuration. 4-AP sensitive currents were isolated by adding 1 µM of the sodium (Na^+) current blocker tetrodotoxin (TTX) (Tocris), 10 mM of the slow activating, non-inactivating K^+ current blocker tetraethylammonium chloride (TEA-Cl) (Millipore-Sigma), and 0.5 mM of the non-selective Ca^{2+} current blocker nickel (II) chloride ($NiCl_2$) (Millipore-Sigma), to ACSF (baseline conditions). Since I_A and I_D have different sensitivities to 4-AP, 3 mM of 4-AP (Tocris) was added to block I_A and 40 µM of 4-AP was added to block I_D. 4-AP was perfused along with the abovementioned baseline channel inhibitors, then current response from the same cell was recorded ≥ 5 min after drugs application to ACSF. Change in net I_A and I_D currents was calculated by subtracting current values in the respective presence of 3 mM and 40 µM 4-AP from values during baseline conditions. For each voltage input step, current recordings were repeated a minimum of three times, and average output values were plotted versus voltage inputs to generate current-voltage (I-V) graphs. Specific quantification values for electrophysiology data are reported in Table S2 [see Additional file 2].

3.10. Experimental design and statistical analysis

OCHSCs obtained from each animal were divided into different experimental groups, with each group being randomly assigned 1–2 OCHSCs. For electrophysiological and imaging data, each experimental

group included a minimum of 3 brain slices derived from a minimum of 2 different animals, and each animal was from a separate litter. Electrophysiological data was analyzed using Clampfit 10.4 (Molecular Devices). Only one neuron per OCHSC was recorded and included in the analysis. Semi-quantification of confocal images was performed on composite image stacks, with regions of interest demarcated in individual focal planes in separate channels. Threshold was automatically set using default settings, background was subtracted, signals were normalized and values were averaged for the same region. All images were processed through LAS X (version 3.1.5), and analyzed using FIJI (ImageJ, NIH, Bethesda, MD). Statistics and graphs were produced using GraphPad Prism 5.0 (GraphPad Software). When applicable, normality of data distribution was assessed with D'Agostino & Pearson test. Differences between three or more experimental groups were assessed with one-way ANOVA followed by Bonferroni post hoc comparison. I_D and I_A differences were determined between three or more groups by repeated measures one-way ANOVA followed by Bonferroni post hoc comparison. All results are expressed as mean ± standard error of mean (SEM), with n being the number of neurons analyzed. Mean differences were considered to be significant at $p < 0.05$. Schematic illustrations were created with BioRender online platform (https://biorender.com).

4. Results

4.1. Direct contact between PBMCs and OCHSC cortical tissue triggers PBMC motility and translocation through cortical layers to the hippocampus

To identify potential inflammatory effects of PBMCs on cortical and hippocampal cells, OCHSCs prepared from P9/P10 rats were co-cultured with PBMCs extracted from the spleen at the same age. Since rats used in this study were obtained from an outbred rodent stock, OCHSCs and PBMCs were harvested from the same animal in order to reduce alloreactive T lymphocyte recognition of non-self major histocompatibility complex variants present in cells derived from other animals. Before adding PBMCs to OCHSCs, PBMCs were primed using the TLR4 ligand LPS (signal 1) (14), then exposed to the K^+ antiporter nigericin, which depletes intracellular K^+ concentration (signal 2) (9, 14), thereby fully activating the NLRP3 inflammasome. PBMCs were divided into three groups: 1) PBMCs stimulated by sequential incubation of LPS and nigericin, hereafter referred to as immunoreactive PBMCs (IR-PBMCs), 2) primed PBMCs stimulated by LPS only (LPS-PBMCs), and 3) untreated PBMCs (control PBMCs). OCHSC-PBMC co-culture groups were compared to naive OCHSCs (Fig. 1). Because different peripheral cell types can penetrate the blood-brain barrier and have the capacity to induce neuroinflammation upon extravasation (4, 5, 27, 28), we opted to include all splenic PBMC subtypes in our study rather than using a subset of purified cell types.

We first investigated the efficacy of the OCHSC-PBMC co-culture model by evaluating potential PBMC invasion of cortical and hippocampal layers upon seeding of PBMCs on top of cortical layer I of OCHSCs. Using pre-labeled control PBMCs with the fluorescent CFSE dye, we traced transmigration of PBMCs 2 hours after seeding them onto OCHSCs (Fig. 2). Transmigration of CFSE-labeled ($CFSE^+$) cells was detected throughout the entire OCHSC, spreading across different cortical (Fig. 2C and E), and

hippocampal layers (Fig. 2C and F). Further, localization of PBMCs was not limited to superficial sections of OCHSCs, but cells were also found in deep tissue sections irrespective to the OCHSC region, thus, suggestive of the formation of cell-adhesion between PBMCs and neural cells.

We next exploited the semi-porous properties of the membrane insert, which is at an interface between OCHSCs and culture media, to assess the effect of cytokine infiltration on neuronal function independently from PBMC trafficking. We compared a) adding $CFSE^+$ PBMCs on top of OCHSCs, where PBMCs are in direct contact with brain-derived tissue, to b) wherein $CFSE^+$ PBMCs were added solely to the media. In contrast to OCHSC-PBMC direct co-culture, no fluorescent cells were observed in OCHSCs when PBMCs were added to the media (Fig. 2D, G and H), thus showing that the membrane is impervious to PBMCs, and appears to effectively recapitulate some aspects of the blood-brain barrier by protecting OCHSCs from PBMC infiltration.

These findings denote that PBMCs retain their motility in vitro, with the capacity to crawl towards the cortex and the hippocampus upon the establishment of cell-cell contact between themselves and OCHSC tissue. Moreover, when PBMCs are applied to the media, the semi-porous membrane acts as a physical barrier isolating OCHSCs from PBMCs.

4.2. The hippocampus is more susceptible to PBMC-induced neuroinflammation than the cortex

PBMCs can transduce peripheral inflammatory signals to the CNS via secretory pro-inflammatory cytokines, such as IL-1β and IL-18, which can trigger neuroinflammation by binding to cognate receptors on the surface of neuronal and glial cells (e.g. IL-1R1 and IL-1R5) (29). Since exposure to both LPS and nigericin is required for activation of Caspase-1 (11, 12, 14), pro-inflammatory cytokine release should be restricted to the two-signal activated IR-PBMCs, whereas LPS-PBMCs (signal 1 only) and control PBMCs, lack the capacity for cytokine production. Importantly, pro-inflammatory cytokines such as IL-1β, that are released following NLRP3 inflammasome activation can in turn serve as a signal 1 to prime neighbouring IL-1R1-expressing cells (30).

To verify potential cytokine-mediated transduction of peripheral inflammation to neural tissue when PBMCs come into close proximity with OCHSCs, we used semi-quantitative immunohistochemical analysis to characterize the expression profile of inflammasome markers, such as NLRP1 and NLRP3, in cortical and hippocampal OCHSC tissue. Immunolabeling of NLRP1 revealed that adding IR-PBMCs to OCHSCs resulted in NLRP1 induction in both cortical (Fig. 3J) and hippocampal cells (Fig. 4J) compared to naive OCHSCs (cortex, Fig. 3A; hippocampus, Fig. 4A). However, this trend was significant only in the hippocampus (cortex, Fig. 3M, $p = 0.08$; hippocampus, Fig. 4M, $p < 0.01$; one-way ANOVA). Surprisingly, following the administration of LPS-PBMCs, NLRP1 was significantly upregulated in the hippocampus (Fig. 4G and M; $p < 0.05$; one-way ANOVA), but not in the cortex (Fig. 3G and M; $p = 0.26$; one-way ANOVA) of OCHSCs, suggesting that immunologically primed PBMCs are capable of transducing peripheral inflammation to hippocampal cells. Conversely, NLRP1 was absent in the cortex (Fig. 3D and M; $p > 0.99$;

one-way ANOVA) and hippocampus (Fig. 4D and M; $p > 0.99$; one-way ANOVA) of OCHSCs co-cultured with control PBMCs.

Next, we analyzed NLRP3 expression in OCHSCs. Similar to NLRP1 immunostaining results, we found NLRP3 immunoreactive cells in the cortex and the hippocampus of IR-PBMC-OCHSC co-cultures (cortex, Fig. 3K and N, $p < 0.001$; hippocampus, Fig. 4K and N, $p < 0.0001$, one-way ANOVA). However, NLRP3 was markedly upregulated in both the cortex (Fig. 3H and N; $p < 0.01$; one-way ANOVA) and the hippocampus (Fig. 4H and N; $p < 0.01$; one-way ANOVA) of LPS-PBMC-OCHSC co-cultures as opposed to naive OCHSCs (cortex, Fig. 3B and N; hippocampus, Fig. 4B and N). Thus, unlike NLRP1 inflammasomes, NLRP3 inflammasomes can be activated in CNS cells upon exposure to LPS-PBMCs. On the other hand, NLRP3 was neither detectable in the cortex (Fig. 3E and N; $p > 0.99$; one-way ANOVA) nor in the hippocampus (Fig. 4E and N; $p > 0.99$; one-way ANOVA) when control PBMCs were added to OCHSCs.

A signature aspect of NLRP1 and NLRP3 inflammasome assembly and maturation is activation of the scaffolding protein ASC (31), however, NLRP1 can also promote inflammasome assembly independent of ASC by interacting directly with Caspase-1 (32). Therefore, we next investigated potential enhancement of ASC synthesis in OCHSCs following LPS- and IR-PBMCs application to OCHSCs. ASC was notably elevated in both the cortex and the hippocampus upon co-culturing OCHSCs with IR-PBMCs (cortex, Fig. 3L, L´ and O; hippocampus, 4L, L´ and O) and LPS-PBMCs (cortex, Fig. 3I, I´ and O; hippocampus, 4I, I´ and O) as compared to the cortex and hippocampus of control PBMC-OCHSC co-cultures (cortex, Fig. 3F, F´ and O; hippocampus, 4F, F´ and O) (IR-PBMCs: cortex, $p < 0.01$, hippocampus, $p < 0.001$; LPS-PBMCs: cortex, $p < 0.01$, hippocampus, $p < 0.01$, one-way ANOVA) and naive OCHSCs (cortex, Fig. 3C, C´ and O; hippocampus, Fig. 4C, C´ and O) (IR-PBMCs: cortex, $p < 0.05$, hippocampus, $p < 0.01$; LPS-PBMCs: cortex, $p < 0.05$, hippocampus, $p < 0.05$; one-way ANOVA). Hence, ASC expression was only detected when NLRP3 was also expressed.

Altogether, analysis of inflammasome induction in OCHSCs indicates that signal 1 priming of PBMCs via LPS, irrespective of signal 2 activation, was sufficient to transduce peripheral pro-inflammatory signals to OCHSCs, which is manifested by activation of inflammasome cascades in cortical and hippocampal cells. Nevertheless, expression of inflammasome proteins was more pronounced in the hippocampus than in the cortex. Additionally, adding control PBMCs to OCHSCs appears to be innocuous, as there was no NLRP1 or NLRP3 inflammasome recruitment in either the cortex or the hippocampus.

4.3. Transduction of peripheral inflammation to neural tissue is coupled with hyperexcitability in pyramidal neurons

To address whether peripheral inflammation transduced to OCHSCs gives rise to functional changes in cortical and hippocampal neurons, we measured neuronal excitability by performing whole-cell electrophysiological recordings in pyramidal neurons in cortical layer II/III and in the CA1 region of the hippocampus.

Cortical pyramidal neurons from all experimental PBMC-OCHSC groups, i.e. control PBMCs, LPS-PBMCs and IR-PBMCs, showed similar resting membrane potential values to naive OCHSCs (Table S2; $p = 0.59$,

one-way ANOVA). In addition, we found no change in cortical cell membrane capacitance (C_m) between OCHSCs incubated with all PBMC groups and naive OCHSCs (Table S2; $p = 0.69$, one-way ANOVA) or in the duration of action potential repolarization (APR) exhibited by cortical neurons between OCHSCs incubated with all PBMC groups and naive OCHSCs (Fig. 3R and U; $p = 0.82$, one-way ANOVA). However, compared to naive OCHSCs, adding IR-PBMCs and LPS-PBMCs to OCHSCs significantly increased the input resistance (R_{in}) of cortical neurons (Fig. 3P and S; $p < 0.05$, $p < 0.01$, respectively, one-way ANOVA), whereas there was no change after adding control PBMCs (Fig. 3P and S; $p > 0.99$; one-way ANOVA). This increase of R_{in} after adding IR-PBMCs was significantly higher than that measured after adding control PBMCs (Fig. 3P and S; $p < 0.05$; one-way ANOVA). Furthermore, while the rheobase of cortical neurons was significantly lower in the IR-PBMC-OCHSC co-culture group versus naive OCHSC and control PBMCs groups (Fig. 3Q and T; $p < 0.05$ and $p < 0.05$, respectively, one-way ANOVA), the rheobase of cortical neurons after adding LPS-PBMCs and control PBMCs was comparable to those of naive OCHSCs (Fig. 3Q and T; $p > 0.99$ and $p > 0.99$, respectively; one-way ANOVA).

Hence, following the application of control, LPS- or IR-PBMCs, cortical neurons did not display noticeable electrophysiological alterations with respect to resting membrane potential, C_m or APR. Yet, co-culturing of LPS- and IR-PBMCs did induce R_{in} changes in cortical neurons. Interestingly, only the addition of IR-PBMCs produced changes in action potential firing propensity, i.e. rheobase, whereas the addition of LPS-primed PBMCs had no effect on cell firing.

Recordings from hippocampal pyramidal neurons were, for the most part, analogous to their cortical counterparts, since there were no notable differences between naive OCHSCs and OCHSCs co-cultured with any of the PBMC groups with respect to resting membrane potential (Table S2; $p = 0.75$; one-way ANOVA), or C_m (Table S2; $p = 0.50$, one-way ANOVA). Also, similar to cortical neurons, hippocampal neurons exhibited significantly augmented R_{in} after seeding of IR-PBMCs and LPS-PBMCs on OCHSCs (Fig. 4P and S; $p < 0.001$ and $p < 0.001$, respectively, one-way ANOVA) relative to naive OCHSCs, and this augmentation was significant for both groups when compared to control PBMCs (Fig. 4P and S; IR-PBMCs: $p < 0.001$, LPS-PBMCs: $p < 0.001$; one-way ANOVA), which was not significantly different from naive OCHSCs (Fig. 4P and S; $p > 0.99$; one-way ANOVA).

In terms of cell firing, application of IR-PBMCs to OCHSCs resulted in rheobase reduction versus control PBMCs and naive OCHSCs (Fig. 4Q and T; $p < 0.01$ versus naive OCHSCs, $p < 0.01$ versus control PBMCs, one-way ANOVA). Also, there was no significant difference between control PBMC-OCHSC co-cultures and naive OCHSC (Fig. 4Q and T; $p > 0.99$; one-way ANOVA). Conversely, unlike cortical pyramidal neurons, following LPS-PBMCs application, the rheobase of hippocampal neurons was markedly reduced compared to control PBMCs (Fig. 4Q and T; $p < 0.01$; one-way ANOVA) and naive OCHSCs (Fig. 4Q and T; $p < 0.01$; one-way ANOVA). Thus, in contrast to the cortex, the effect of LPS-primed PBMCs on rheobase in the hippocampus was reminiscent to IR-PBMCs, where both groups elicited comparable hyperexcitability in OCHSCs when compared to the control groups.

Likewise, APR was notably extended in hippocampal pyramidal neurons recorded following IR-PBMCs and LPS-PBMCs incubation, when compared to control PBMCs incubation and naive OCHSCs (Fig. 4R and U; IR-PBMCs: $p < 0.05$ versus naive OCHSCs, $p < 0.05$ versus control PBMCs; LPS-PBMCs: $p < 0.05$ versus naive OCHSCs, $p < 0.01$ versus control PBMCs, one-way ANOVA), with no significant change between naive OCHSCs and OCHSCs co-cultured with control PBMCs (Fig. 4R and U; $p > 0.99$; one-way ANOVA). Accordingly, unlike the cortex where none of the PBMC groups had any effect on APR, LPS- and IR-PBMCs generated APR extension in hippocampal neurons, which indicates different action potential kinetics between cortical and hippocampal neurons.

Taken together, upon application on OCHSCs, both LPS- and IR-PBMCs altered some of the intrinsic properties of cortical and hippocampal pyramidal neurons associated with excitability. Notably, enhancement of neuronal excitability correlates with the expression of NLRP1 and/or NLRP3 inflammatory markers in OCHSCs.

4.4. Activation of inflammasomes in OCHSCs promotes a decline in 4-AP sensitive transient K^+ currents in pyramidal neurons

The reduction of rheobase and prolongation of the repolarization duration in pyramidal neurons after exposure to PBMCs is likely to arise from changes in the properties of specific ion channels that are activated when graded potential reaches threshold potential as well as during the repolarization phase. Thus, we next asked which ion channels would satisfy these criteria.

Interestingly, transient A-type fast activating, fast inactivating voltage-dependent K^+ current (I_A) is known to regulate action potential rheobase and waveform (33–35). In addition, LPS incubation with caudate nucleus cultures has been shown to reduce I_A *in vitro* (36). Therefore, we postulated that suppression of I_A might be a plausible culprit underlying neuronal excitability changes elicited by inflammation. To explore putative suppression of I_A in OCHSCs, we obtained whole-cell recordings while blocking Na^+, Ca^{2+} currents together with the majority of K^+ currents (also referred to as baseline conditions), then repeated the same recordings again while adding 3 mM of 4-AP to the abovementioned current blockers to selectively inhibit I_A (Fig. 5F). Net I_A was derived by calculating current difference between both conditions.

I_A in cortical neurons was notably abrogated in the IR-PBMCs group versus naive OCHSCs (Fig. 5A, B and E; $p < 0.01$; repeated measures one-way ANOVA) and control PBMCs groups (Fig. 5E; $p < 0.001$; repeated measures one-way ANOVA), whereas cortical neurons in the LPS-PBMCs and control PBMCs groups showed similar I_A activation to naive OCHSCs (Fig. 5E; $p > 0.99$ and $p = 0.82$, respectively; repeated measures one-way ANOVA). On the other hand, adding either IR-PBMCs or LPS-PBMCs to OCHSCs substantially reduced I_A in hippocampal neurons relative to naive OCHSCs (Fig. 5C, D and G; IR-PBMCs: $p < 0.001$; LPS-PBMCs: $p < 0.0001$; repeated measures one-way ANOVA) and to control PBMCs (Fig. 5G; IR-PBMCs: $p < 0.0001$; LPS-PBMCs: $p < 0.0001$; repeated measures one-way ANOVA). Markedly, the effect of

co-culturing control PBMCs with OCHSCs was opposite to LPS- and IR-PBMCs, resulting in potentiation of I_A amplitude compared to naive OCHSCs (Fig. 5G; $p < 0.0001$; repeated measures one-way ANOVA).

Beside I_A, we also considered other potential ion channel candidates influenced by PBMC-induced neuroinflammation. Given that transient D-type fast activating, slowly inactivating voltage-dependent K^+ current (I_D) is sensitive to 4-AP much like I_A, and activation of I_D delays action potential firing along with reducing action potential duration in pyramidal neurons (33, 35, 37, 38), we decided to investigate the possible contribution of I_D in inflammation-induced excitability. However, while 4-AP inhibits I_A activation in millimolar concentrations, (1–3 mM), I_D is highly sensitive to 4-AP, i.e. in micromolar concentrations (30–100 μM) (33–35, 37). Therefore, we isolated I_D using the same approach as I_A, except the concentration of 4-AP was 40 μM, instead of 3 mM (Fig. 5M).

Results from pyramidal neurons in the cortex revealed that relative to naive OCHSCs, the amplitude of I_D was significantly diminished only when OCHSCs were co-cultured with IR-PBMCs (Fig. 5H, I and L; $p < 0.01$; repeated measures one-way ANOVA), whereas there were no significant changes in I_D amplitude upon co-culturing OCHSCs with control PBMCs (Fig. 5H; $p = 0.08$) ; repeated measures one-way ANOVA or LPS-PBMCs (Fig. 5H; $p = 0.35$; repeated measures one-way ANOVA). In hippocampal neurons, OCHSCs co-cultured with IR-PBMCs and LPS-PBMCs showed significantly lower I_D than naive OCHSCs (Fig. 5J, K and N; IR-PBMCs: $p < 0.0001$; LPS-PBMCs: $p < 0.0001$; repeated measures one-way ANOVA) as well as control PBMC-OCHSC co-cultures (Fig. 5N; IR-PBMCs: $p < 0.0001$; LPS-PBMCs: $p < 0.001$; repeated measures one-way ANOVA), whereas adding control PBMCs did not result in significant changes in I_D compared to naive OCHSCs (Fig. 5N; $p = 0.06$; repeated measures one-way ANOVA).

Collectively, changes in I_A and I_D are in line with our previous data, where decay of I_A and I_D was only detected in pyramidal neurons that exhibited changes in cell firing associated with inflammasome induction, i.e. the cortex of IR-PBMC-OCHSC co-cultures and the hippocampus of IR-PBMC- and LPS-PBMC-OCHSC co-cultures.

4.5. Direct cell-cell contact between PBMCs and OCHSCs is required for pro-inflammatory signal transduction from LPS-primed PBMCs to brain-derived tissue

To gain further insight into how pro-inflammatory PBMCs can transduce peripheral inflammation to OCHSCs, we investigated whether diffusible factors secreted by PBMCs, primarily cytokines and chemokines, can mediate inflammation transduction solely by binding to their cognate receptors found in OCHSC cells (29). Since we have demonstrated that when PBMCs were added to the media, the membrane insert acts as a barrier by preventing cell-cell adhesion between PBMCs and OCHSCs (see Sect. 4.1, Fig. 2), we added PBMCs to OCHSC media to allow PBMC-derived cytokines and chemokines, but not PBMCs themselves, to diffuse through the membrane. In the next set of experiments, we focused on the effects of media-incubated PBMCs on inflammasome assembly and neuronal excitability in the hippocampus.

Immunohistochemical analysis of the inflammasome markers NLRP1, NLPR3 and ASC in OCHSCs revealed that media incubation of IR-PBMCs (mIR-PBMCs) gave rise to a stark upregulation of NLRP1 (Fig. 6G and J; $p < 0.0001$; one-way ANOVA), NLRP3 (Fig. 6H and K; $p < 0.01$) and ASC (Fig. 6I, I´ and L; $p < 0.001$; one-way ANOVA) in the hippocampus. On the other hand, while NLRP1 was overexpressed following media incubation of LPS-PBMCs (mLPS-PBMCs) (Fig. 6D and J; $p < 0.05$; one-way ANOVA), there was a non-significant trend of NLRP3 upregulation (Fig. 6E and K; $p = 0.07$; one-way ANOVA) and no detectable expression of ASC (Fig. 6F, F´ and L; $p > 0.99$; one-way ANOVA) as compared to media incubation of control PBMCs (mCTL-PBMCs) (Fig. 6A-C´ and J-L). In addition, the expression level of NLRP1 and ASC, but not NLRP3, was significantly higher when OCHSCs were incubated with mIR-PBMCs than with mLPS-PBMCs (Fig. 5J, K and L; NLRP1: $p < 0.05$, NLRP3: $p = 0.42$, ASC: $p < 0.01$; one-way ANOVA). The presence of NLRP1/3 inflammasomes scaffolding protein ASC in the mIR-PBMCs group supports the hypothesis that IR-PBMCs can induce inflammasome oligomerization in OCHSCs through diffusible mediators, whereas the failure of mLPS-PBMCs to evoke similar effect suggests that LPS-PBMCs require cell-cell contact with neural tissue for inflammasome activation.

Following media incubation of all experimental PBMC groups, the values of R_{in}, rheobase and APR in hippocampal pyramidal neurons exposed to mLPS-PBMCs were reminiscent to hippocampal neurons exposed to mCTL-PBMCs (Fig. 5P-R; R_{in}: $p = 0.41$, rheobase: $p = 0.93$, APR: $p > 0.99$; one-way ANOVA), and consistent with the absence of hippocampal inflammasome activation in OCHSCs following mLPS-PBMCs. However, in hippocampal neurons exposed to mIR-PBMCs, R_{in}, rheobase and APR values were significantly different from mCTL-PBMCs (Fig. 5M-R; R_{in}: $p < 0.01$, rheobase: $p < 0.05$, APR: $p < 0.05$; one-way ANOVA), again consistent with inflammasome induction in OCHSCs from this group. Hence, in contrast to adding LPS-PBMCs on top of OCHSCs (Sect. 4.3, Fig. 4S-U), the outcome of mLPS-PBMCs was comparable to that of mCTL-PBMCs, indicating that media application of LPS-PBMCs was sufficient to enhance neuronal excitability. Also, these results demonstrate that similar to IR-PBMCs, mIR-PBMCs retained their capacity to enhance neuronal excitability.

Furthermore, the difference of the amplitude of the 4-AP sensitive I_A and I_D between hippocampal neurons of OCHSCs incubated with mLPS-PBMCs and those incubated with mCTL-PBMCs was not significant (Fig. 5T and V; I_A: $p > 0.99$, I_D: $p > 0.99$; repeated measures one-way ANOVA). Still, both I_A and I_D amplitudes were significantly lower in hippocampal neurons when OCHSCs were incubated with mIR-PBMCs as opposed to those incubated with mCTL-PBMCs (Fig. 5S-V; I_A: $p < 0.01$, I_D: $p < 0.05$; repeated measures one-way ANOVA) and mLPS-PBMCs (Fig. 5T and V; I_A: $p < 0.01$, I_D: $p < 0.01$; repeated measures one-way ANOVA). The fact that a significant decrease of amplitude of I_A and I_D was present only in the mIR-PBMCs group further confirms the correlation between PBMC-induced hyperexcitability and changes in these 4-AP sensitive currents.

In summary, with respect to the hippocampus, mIR-PBMCs mirrored the effects of co-culturing IR-PBMCs with OCHSCs, reproducing inflammasome formation and I_D-/I_A-mediated hyperexcitability, thereby suggesting that diffusion of inflammatory factors secreted by mIR-PBMCs, likely cytokines, rather than

cell-cell contact is responsible of these phenotypic changes observed in OCHSCs. On the contrary, mLPS-PBMCs unexpectedly failed to provoke inflammasome assembly or neuronal hyperexcitability; an outcome that was distinct from LPS-PBMC-OCHSC co-cultures. Thus, in the case of LPS-PBMCs, cell-cell contact seems to be essential for transducing peripheral inflammatory signals from LPS-PBMCs to the hippocampus in OCHSCs.

4.6. Neuroinflammation-mediated attenuation of 4-AP sensitive transient K^+ currents is dependent on Caspase-1 activation in hippocampal cells

Pharmacological inhibition of Caspase-1 cleavage using the selective inhibitor VX-765 has proved to be highly effective in reducing inflammasome activation in the CNS (39–41). To test if Caspase-1 inhibition could mitigate PBMC-induced neuroinflammation in the hippocampus, OCHSCs were pre-treated with VX-765 one hour before seeding LPS-PBMCs (VX765-LPS-PBMCs) and IR-PBMCs (VX765-IR-PBMCs) on top of OCHSCs. Thereafter, we analyzed the expression profile of inflammasome markers and measured neuronal excitability following the co-culturing of PBMCs with OCHSCs. Because VX-765 was dissolved in DMSO, we pre-treated OCHSCs with DMSO, i.e. the vehicle, one hour prior to applying LPS-PBMCs (DMSO-LPS-PBMCs) and deemed this group as the control group.

We found notable augmentation of NLRP1, NLRP3 and ASC immunolabeling in the DMSO-LPS-PBMCs group (Fig. 7A-C´ and J-L) as opposed to the VX765-LPS-PBMCs (Fig. 7D-F´ and J-L; NLRP1: $p < 0.01$, NLRP3: $p < 0.01$, ASC: $p < 0.001$; one-way ANOVA) and the VX765-IR-PBMCs groups (Fig. 7G-I´ and J-L; NLRP1: $p < 0.01$, NLRP3: $p < 0.001$, ASC: $p < 0.001$; one-way ANOVA). Thus, VX-765 is a potent inhibitor of PBMC-transduced inflammatory signals in OCHSC hippocampal tissue.

In addition, patch-clamp recordings showed that hippocampal pyramidal neurons displayed significantly lower R_{in}, lower rheobase and slower APR in DMSO-LPS-PBMC co-cultures relative to VX765-LPS-PBMC (Fig. 7M-R; R_{in}: $p < 0.01$, rheobase: $p < 0.05$, APR: $p < 0.05$; one-way ANOVA) and VX765-IR-PBMC co-cultures with OCHSCs (Fig. 7M-R; R_{in}: $p < 0.05$, rheobase: $p < 0.05$, APR: $p < 0.05$; one-way ANOVA). Further, I_A and I_D amplitudes of hippocampal neurons from DMSO-LPS-PBMC co-cultures were notably reduced versus VX765-LPS-PBMC (Fig. 7S-V; I_A: $p < 0.001$, I_D: $p < 0.001$; repeated measures one-way ANOVA) and VX765-IR-PBMC co-cultures with OCHSCs (Fig. 7S-V; I_A: $p < 0.01$, I_D: $p < 0.05$; repeated measures one-way ANOVA).

Taken together, this data provides evidence that in the hippocampus, VX-765 treatment reversed the hyperexcitability concurrent with neuroinflammation triggered by pro-inflammatory PBMCs, therefore implicating Caspase-1–dependent pathway(s) as an underlying mechanism of PBMC-induced I_A- and I_D-mediated enhanced excitability.

5. Discussion

It has been previously demonstrated that induction of innate immunity outside of the CNS, i.e. peripheral inflammation, promotes neuroinflammation, which may subsequently lead or contribute to pathophysiological disorders within the CNS, including epilepsy (1, 42). More recently, inflammasomes have been found to contribute to the initiation of innate immune response, including release of pro-inflammatory cytokines and pyroptotic cell death, (43), and a growing body of research suggests that inflammasomes constitute viable therapeutic targets (44). In order to delineate the mechanisms that activate inflammasomes in the brain following PBMC extravasation, in this study, we co-cultured activated PBMCs with OCHSCs, and compared activated PBMCs, i.e. IR-PBMCs, and primed PBMCs, i.e. LPS-PBMCs, with naive PBMCs that were not exposed to inflammatory stimulants. Collectively, the data presented herein demonstrates that triggering inflammasome formation in PBMCs results in neuronal hyperexcitability upon PBMC encounter with CNS tissue, thus, suggesting that inflammasome activation in peripheral immune cells has pathogenic implications on the brain. A second significant finding here is that the hippocampus is more prone to the pro-excitant effects of systemic inflammation than the cortex. In addition, we provide new evidence that I_A and I_D are downstream targets of Caspase-1-activating inflammasomes.

Using the PBMC-OCHSC co-culture model in conjunction with fluorescent live-cell labeling of PBMCs, we revealed that naive PBMCs have the capacity to adhere to OCHSCs, which denote potential immunological crosstalk between PBMCs and neural cells. Yet, because the fluorescent dye used was not specific to certain PBMC subpopulations, we could not identify whether cell-cell contact was established between all or only some peripheral cell subtypes and brain-derived tissue. Future studies should unveil the identity of neuronal/glial cells and PBMC subtypes that establish cell-cell adhesion in our model. In contrast, adding PBMCs solely to the media failed to result in PBMC adherence to OCHSC tissue as the membrane inset prevented infiltration of media-incubated PBMCs. This attribute of the interface culture system allowed us to compare the outcome of culturing inflammatory PBMCs in direct contact with OCHSCs, with that of culturing inflammatory PBMCs in the media in isolation from OCHSCs, in our studies.

When PBMCs were co-cultured in direct contact with OCHSCs, there were evident differences between the cortex and the hippocampus. While IR-PBMCs triggered NLRP3 inflammasome formation and pro-excitable changes (R_{in}, rheobase, I_A and I_D) in cortical and hippocampal tissues, NLRP1 expression induced by IR-PBMCs was only displayed by the hippocampus. Furthermore, LPS-PBMCs triggered NLRP1, NLRP3 and ASC expression and altered neuronal excitability (rheobase, I_A and I_D) only in the hippocampus. Thus, these findings suggest that the hippocampus was more vulnerable to co-culturing of LPS-PBMCs than the cortex. Interestingly, a previous report also found that systemic administration of LPS *in vivo* rendered the hippocampus more susceptible to neuroinflammation than the cortex (45). One explanation of this phenomenon could be ascribed to the relatively high expression of IL-1 receptors in the hippocampus, specifically the dentate gyrus, compared to other structures like the cortex, which leads to higher sensitivity to IL-1 cytokines, including IL-1β (46–48). Notably, untreated PBMCs failed to induce neuroinflammation. This finding is corroborated by a previous report indicating that lymph-node-derived

lymphocytes not only failed to induce toxicity when incubated with brain-derived organotypic slice cultures *in vitro*, but they were neuroprotective against neurotoxicity (49). Nevertheless, one caveat in our experimental design is that culturing PBMCs over several days, i.e. 6 DIV, prior to adding them to OCHSCs could lead to changes in the proportion of different PBMC subtypes. However, this limitation was inevitable in our model mainly because co-culturing brain slices and PBMCs from the same animal was essential to reduce alloreactivity of T-lymphocytes, and OCHSCs require at least 4–5 DIV to return to their resting ramified state. Furthermore, our electrophysiological and immunohistochemical results indicate that the variability between replicates within the same experimental group was relatively low, which suggests that any potential transformation in PBMC composition was minimal during culturing.

Adding IR-PBMCs to the media, i.e. mIR-PBMCs, provoked inflammasome formation and hyperexcitability in hippocampal neurons in the same fashion as adding IR-PBMCs directly on top of OCHSCs. These results favor the notion that inflammatory transduction was achieved via binding of cytokines released by IR-PBMCs to their cognate receptors in the hippocampus. In addition, because mIR-PBMCs have no contact with OCHSCs, the comparable expression profile of inflammasome markers NLRP1, NLRP3 and ASC after adding IR-PBMCs and mIR-PBMCs to OCHSCs indicates the inflammasomes detected in OCHSC-IR-PBMCs are not likely localized within PBMCs. Lack of co-localization between the pan-neuronal marker NeuN and any of the inflammasome markers suggests that inflammasome formation in OCHSCs was due to glial cells rather neurons. Microglia and/or astrocytes convey peripheral inflammatory signals to neurons possibly via releasing gliotransmitters, such as ATP or glutamate, thus leading to neuronal hyperexcitability (50). On the other hand, media application of LPS-PBMCs, i.e. mLPS-PBMCs, stimulated NLRP1 receptors in OCHSCs, but failed to yield NLRP3 stimulation, inflammasome activation or enhance neuronal excitability in the hippocampus. Hence, NLRP1 stimulation alone in OCHSCs is not sufficient to elicit ASC upregulation or hyperexcitability in the hippocampus, whereas NLRP3 stimulation is likely to be required to induce such aberrant effects. However, it is still unclear whether these effects are mediated by NLRP3 activation alone or in combination with NLRP1. Failure of mLPS-PBMC application to induce ASC upregulation or neuronal hyperexcitability in OCHSCs also indicates that activation of NLRP3 inflammasomes in the hippocampus was dependent on the interaction of PBMCs with OCHSC cells. This cell-cell interaction requirement for LPS-PBMCs to transduce peripheral pro-inflammatory signals to neural tissue suggests that despite LPS-PBMCs having the capacity to secrete pro-inflammatory cytokines, priming of PBMCs was not sufficient to initiate signal 2 in NLRP3 inflammasome signaling pathway. This opens the question to how LPS-PBMCs added on top of OCHSCs promote inflammasome activation in the hippocampus? It has been previously shown that when brain-derived slices are cultured *in vitro*, they display necrotic cell death up to 6 DIV (51). Of note, necrosis is known to trigger the release of heat shock proteins, which can give rise to innate immunity cascades, like nuclear factor κB signaling pathway (52). Swaroop et al. reported that *in vitro* overexpression of heat shock proteins, specifically the endogenous TLR4 agonist Hsp60, triggers the activation of NLRP3 inflammasome downstream targets, including Caspase-1 (53). Therefore, it is conceivable that heat shock proteins released by OCHSC tissue, e.g. Hsp60, could act as signal 2 to

initiate Caspase-1 cleavage in signal-1-primed cells, i.e. LPS-PBMCs, and thus resulting in inflammasome activation in LPS-PBMCs.

I_A and I_D are voltage-gated delayed rectifying K^+ channels (K_v) that become active at voltages close to action potential threshold, and known to dampen excitation and intrinsically shape action potential waveform (35). Although the identity of the molecular K_v subunits that comprise I_A and I_D is not fully defined, I_D is believed to be mediated by α-dendrotoxin sensitive K_v1 subunits, i.e. $K_v1.1$, $K_v1.2$ and $K_v1.6$, which in addition to being found at the soma and proximal dendrites, are strongly expressed in the axonal initial segment (54, 55). In contrast, I_A is a somatodendritic current whose density increases with distance from the soma (56) and is presumed to be primarily constituted by the K_v4 subunits $K_v4.1$, $K_v4.2$ and $K_v4.3$ (57). Our data suggests that the inflammasome-associated hyperexcitability exhibited by cortical and hippocampal neurons in OCHSCs is partially mediated by the 4-AP sensitive I_A and I_D hyperpolarizing currents. Several other studies have identified a similar correlation between CNS inflammatory insults and aberrant changes of 4-AP sensitive currents that underlie neuronal hyperexcitability. For example, modeling systemic infections in rats by means of LPS intraperitoneal injections exacerbated 4-AP-induced epileptiform burst discharges in the hippocampus compared to saline (7). In addition, acute insults known to trigger neuroinflammation in rodent models, such as ischemic and traumatic brain injury (58, 59), enhanced seizure susceptibility through reduction of I_A in CA1 pyramidal neurons up to one week following traumatic brain injury insult (60). A separate report found that ischemia-hypoxia increased the firing frequency of dorsal root ganglion neurons, which was provoked by I_D-mediated extension of APR (61). Further studies will establish whether inhibition of I_A and I_D in OCHSC neurons incubated with stimulated PBMCs could lead to lowering network convulsive threshold in the presence of chemoconvulsants, like kainic acid, thus potentially facilitating epileptiform activity.

Although adding IR-PBMCs to OCHSCs in our *in vitro* model produced the same diminishing effect on I_A and I_D amplitude in cortical or hippocampal pyramidal neurons, prolongation of APR was only manifested by hippocampal neurons. This discrepancy in PBMC-induced elongation of action potential waveform between cortical and hippocampal neurons could be attributed to different I_A participation to the total hyperpolarizing current during the repolarization phase in cortical and the hippocampal pyramidal neurons. Indeed, while application of 4 mM of 4-AP to cortical layer II/III pyramidal neurons reportedly resulted in extending APR by ~ 42% (62), CA1 and CA3 hippocampal pyramidal neurons exhibited far more drastic broadening of action potential waveform (CA3: ~310%; CA1: >200%) caused by adding 2-2.5 mM of 4-AP (35, 63), thus, suggesting that inflammation-induced decrease of I_A displayed by cortical neurons had marginal impact on the kinetics of APR compared to that in hippocampal neurons. Future experiments will reveal whether inflammasome activation could induce expression perturbance of the major subunits comprising I_A, i.e. K_v4, and I_D, i.e. K_v1. Inflammasomes could reduce other types of outward currents activated during the repolarization phase, such as K^+ current of the delayed rectification (I_{KDR}) and K^+ currents activated by intracellular Ca^{2+} (I_{KCA}) (64), thus, investigation of

possible inflammation-induced changes of other components of the hyperpolarizing current during pyramidal cell firing is warranted.

In our model, Caspase-1 inhibition counteracted neuroinflammation and hyperexcitability that occurred when stimulated PBMCs were applied to OCHSCs, indicating that peripheral inflammation transduction into CNS cells requires Caspase-1-dependent pathways. Interestingly, inhibition of Caspase-1 was neuroprotective in experimental models of multiple sclerosis and Alzheimer's disease (39, 41). Furthermore, in rheumatoid arthritis and dermatitis animal models, VX-765 attenuated peripheral inflammation by inhibiting PBMCs release of IL-1β and IL-18 (65). Thus, our results are consistent with findings by other groups suggesting that targeting Caspase-1 activation is neuroprotective. In addition, several experimental models have shown that modulation of regulators of IL-1β biosynthesis, chiefly Caspase-1, was detrimental to seizure precipitation. In one study, knocking out *Caspase-1* rendered mice significantly more resistant to seizures (66), while two separate studies reported that knockdown of RNA coding for NLRP1, NLRP3 and Caspase-1 reduced ictogenesis (67, 68). Also, targeting Caspase-1 cleavage, through systemic administration of VX-765 in mice, has been shown to yield anticonvulsant effects during pharmacologically induced seizures (69). Hence, our data is in agreement with other reports demonstrating that pharmacological modulation of inflammasomes is a candidate approach to alleviate hyperexcitability co-morbid with neuroinflammatory response. Notably, we also determined that blockade of Caspase-1 activation prevented I_A- and I_D-mediated hyperexcitability in pyramidal neurons, suggesting that the Caspase-1 activation acts -either directly or indirectly- as a neuromodulator, thereby modifying the activity of membrane ion channels. Whether VX-765 suppressed Caspase-1 activation in OCHSCs or PBMCs remains unclear, and will require further experimentation involving restricting Caspase-1 activation to either OCHSCs or PBMCs. Future studies where OCHSCs derived from Caspase-1 knockout transgenic rodents co-cultured with PBMCs extracted from wild type littermates will further determine the role of Caspase-1 expressed by CNS cells in transduction of peripheral inflammation.

Finally, our findings using the OCHSC-PBMC co-culture model are in line with previously published results that used similar paradigms. Indeed, it has been previously shown that interaction of pro-inflammatory peripheral immune cells with brain-derived slices, whether through an acute *ex vivo* setting or organotypic cultures *in vitro*, establishes cell-cell contact between peripheral-neural cells as well as gives rise to neuroinflammation and aberrant synaptic transmission in brain slices (70–72). It will be important in future experimental work to determine whether specific lymphocytic or myeloid cell subtypes isolated from PBMCs can mediate pathological pro-excitation of pyramidal neurons when co-cultured alone with OCHSCs. Also, inhibition of IL-1 pathway in OCHSC-PBMC co-cultures, e.g. via administration of exogenous IL-1 receptor antagonist (or anakinra) (73), would verify whether pro-inflammatory cytokines released by IR-PBMCs, namely IL-1β and IL-18, are necessary for PBMC-induced effects. In addition, taking advantage of conditional mutant mouse lines that ablate the expression of inflammasome regulating genes, such as Caspase-1 or ASC, in astrocytes or microglia could help identify potential glial-derived molecular signals that contribute to transduction of peripheral inflammation to neurons.

Overall, the model presented herein provides novel insights into the mechanisms underlying predisposition of neuronal networks to hyperexcitation following an insult extrinsic to the CNS, specifically when inflammatory signals are transduced to the CNS through peripheral immune cells.

6. Conclusion

The main findings of our study show that extravasation of activated peripheral immune cells, such as that which occurs during systemic inflammation, results in aberrant excitability in pyramidal neurons. We found that in the cortex, the effects of peripheral inflammation in immunogenically-primed PBMCs were relatively limited, when compared to immunogenically-activated PBMCs, suggesting that the degree of immune stimulation of infiltrating cells predicates the extent of immune response in cortical cells. In contrast, we show that the hippocampus displayed the same vulnerability to both immunogenically-primed and immunogenically-activated PBMCs, with alteration of neuronal intrinsic properties being comparable between primed and activated PBMCs. Yet, in the case of primed PBMCs, transduction of pro-inflammatory signals seems to be dependent on cell-cell contact between PBMCs and the hippocampal tissue. Finally, by targeting inflammasome activation pharmacologically, we found that inflammation-induced excitation in hippocampal neurons was mediated through Caspase-1 downstream effectors, where Caspase-1 activation results in enhancing neuronal excitability by diminishing 4-AP sensitive K^+ currents that dampen neuronal membrane excitability, namely I_D and I_A. Hence, we provide evidence that Caspase-1 signaling can regulate functional properties of 4-AP sensitive K^+ channels in pyramidal neurons, which might help develop therapeutic approaches targeting Caspase-1 in order to control neuroinflammation and hyperexcitability following systemic infections or injuries.

Abbreviations

4-AP: 4-aminopyridine; **ACSF:** Artificial cerebrospinal fluid; **APR:** Action potential repolarization; **ASC:** Associated speck-like protein containing a carboxy-terminal CARD; **Ca^{2+}:** Calcium; **CFSE:** Carboxyfluorescein diacetate succinimidyl ester; **$CFSE^+$:** CFSE-labeled; **C_m:** Cell membrane capacitance; **CNS:** Central nervous system; **CTL:** Control; **DAPI:** 4',6-diamidino-2-phenylindole; **DIV:** Days *in vitro*; **I_A:** A-type fast activating, fast inactivating voltage-dependent K^+ current; **I_D:** D-type fast activating, slowly inactivating voltage-dependent K^+ current; **I_{KCA}:** K^+ currents activated by intracellular Ca^{2+}; **I_{KDR}:** K^+ current of the delayed rectification; **IL:** Interleukin; **IR:** Immunoreactive; **I-V:** Current-voltage; **K^+:** Potassium; **K_V:** Voltage-gated potassium channels; **LPS:** Lipopolysaccharide; **m:** Media incubation of PBMCs; **Mg^{2+}:** Magnesium; **Na^+:** Sodium; **NLR:** NOD-like receptor; **NLRP3:** NLR Family Pyrin Domain Containing 3; **OCHSCs:** Organotypic cortico-hippocampal brain slice cultures; **P:** Postnatal day; **PBMCs:** Peripheral blood mononuclear cells; **PBS:** Phosphate buffered saline; **Pro-:** Precursor form; **R_{in}:** Input resistance; **SEM:** Standard error of mean; **TLR:** Toll-like receptor.

Declarations

Ethics approval and consent to participate

All procedures involving animals were performed in accordance with institutional policies and guidelines (Protocol #603, CIBPAR, Sainte-Justine Hospital Research Centre, Université de Montréal, Montreal, QC, Canada).

Consent for publication

Not applicable

Availability of supporting data and materials

All data generated or analyzed for this study is included in this published article. Any additional information will be made available by the corresponding author upon request.

Competing interests

The authors declare no competing interests.

Funding

This work was supported by Fondation Charles Guidon pour l'épilepsie (A.G.W.).

Authors' contributions

T.S. conceived, designed and performed most of the experiments. B.C. assisted with immunohistochemistry and performed all confocal imaging. Data was analyzed by T.S. and B.C. The manuscript was written by T.S., with assistance from B.C., and edited by all authors. A.G.W., B.A. and G.D.C. contributed to this work through supervision, equipment, reagents, technical and intellectual assistance. All authors read and approved the final version of the manuscript.

Acknowledgements

We thank Dr. Lionel Carmant at Université de Montréal for helping with experimental design, supervising part of the experiments conducted in this study, and providing funding through Canadian Institutes of Health Research. We thank Dr. William Colmers and Dr. Christopher Power at the University of Alberta (Edmonton, Alberta) for providing insightful input and technical assistance on the conception and design of the project. We thank Dr. Nathalie Sanon and Mr. Abdulrahman Elhassan for technical assistance. We thank Dr. Nathalie Arbour and Dr. Brienne A McKenzie for critical reading of the manuscript.

References

1. Kramer U, Chi CS, Lin KL, Specchio N, Sahin M, Olson H, et al. Febrile infection-related epilepsy syndrome (FIRES): pathogenesis, treatment, and outcome: a multicenter study on 77 children.

Epilepsia. 2011;52(11):1956-65.
2. Dube CM, Brewster AL, Richichi C, Zha Q, Baram TZ. Fever, febrile seizures and epilepsy. Trends Neurosci. 2007;30(10):490-6.
3. Nabbout R. Autoimmune and inflammatory epilepsies. Epilepsia. 2012;53 Suppl 4:58-62.
4. Cusick MF, Libbey JE, Patel DC, Doty DJ, Fujinami RS. Infiltrating macrophages are key to the development of seizures following virus infection. J Virol. 2013;87(3):1849-60.
5. Libbey JE, Kennett NJ, Wilcox KS, White HS, Fujinami RS. Interleukin-6, produced by resident cells of the central nervous system and infiltrating cells, contributes to the development of seizures following viral infection. J Virol. 2011;85(14):6913-22.
6. Galic MA, Riazi K, Pittman QJ. Cytokines and brain excitability. Front Neuroendocrinol. 2012;33(1):116-25.
7. Galic MA, Riazi K, Heida JG, Mouihate A, Fournier NM, Spencer SJ, et al. Postnatal inflammation increases seizure susceptibility in adult rats. J Neurosci. 2008;28(27):6904-13.
8. Becker CE, O'Neill LA. Inflammasomes in inflammatory disorders: the role of TLRs and their interactions with NLRs. Semin Immunopathol. 2007;29(3):239-48.
9. Munoz-Planillo R, Kuffa P, Martinez-Colon G, Smith BL, Rajendiran TM, Nunez G. K(+) efflux is the common trigger of NLRP3 inflammasome activation by bacterial toxins and particulate matter. Immunity. 2013;38(6):1142-53.
10. Cruz CM, Rinna A, Forman HJ, Ventura AL, Persechini PM, Ojcius DM. ATP activates a reactive oxygen species-dependent oxidative stress response and secretion of proinflammatory cytokines in macrophages. J Biol Chem. 2007;282(5):2871-9.
11. Mariathasan S, Monack DM. Inflammasome adaptors and sensors: intracellular regulators of infection and inflammation. Nat Rev Immunol. 2007;7(1):31-40.
12. Bauernfeind FG, Horvath G, Stutz A, Alnemri ES, MacDonald K, Speert D, et al. Cutting edge: NF-kappaB activating pattern recognition and cytokine receptors license NLRP3 inflammasome activation by regulating NLRP3 expression. J Immunol. 2009;183(2):787-91.
13. Martinon F, Burns K, Tschopp J. The inflammasome: a molecular platform triggering activation of inflammatory caspases and processing of proIL-beta. Mol Cell. 2002;10(2):417-26.
14. Mariathasan S, Weiss DS, Newton K, McBride J, O'Rourke K, Roose-Girma M, et al. Cryopyrin activates the inflammasome in response to toxins and ATP. Nature. 2006;440(7081):228-32.
15. DeSena AD, Do T, Schulert GS. Systemic autoinflammation with intractable epilepsy managed with interleukin-1 blockade. J Neuroinflammation. 2018;15(1):38.
16. Liu Z, Xian H, Ye X, Chen J, Ma Y, Huang W. Increased levels of NLRP3 in children with febrile seizures. Brain Dev. 2020.
17. Bilbo SD, Biedenkapp JC, Der-Avakian A, Watkins LR, Rudy JW, Maier SF. Neonatal infection-induced memory impairment after lipopolysaccharide in adulthood is prevented via caspase-1 inhibition. J Neurosci. 2005;25(35):8000-9.

18. Chen YH, Kuo TT, Chu MT, Ma HI, Chiang YH, Huang EY. Postnatal systemic inflammation exacerbates impairment of hippocampal synaptic plasticity in an animal seizure model. Neuroimmunomodulation. 2013;20(4):223-32.
19. Yin P, Li Z, Wang YY, Qiao NN, Huang SY, Sun RP, et al. Neonatal immune challenge exacerbates seizure-induced hippocampus-dependent memory impairment in adult rats. Epilepsy Behav. 2013;27(1):9-17.
20. Reid AY, Riazi K, Campbell Teskey G, Pittman QJ. Increased excitability and molecular changes in adult rats after a febrile seizure. Epilepsia. 2013;54(4):e45-8.
21. Gomez CD, Read J, Acharjee S, Pittman QJ. Early Life Inflammation Increases CA1 Pyramidal Neuron Excitability in a Sex and Age Dependent Manner through a Chloride Homeostasis Disruption. J Neurosci. 2019;39(37):7244-59.
22. Schwarz N, Uysal B, Welzer M, Bahr JC, Layer N, Loffler H, et al. Long-term adult human brain slice cultures as a model system to study human CNS circuitry and disease. Elife. 2019;8.
23. De Simoni A, Griesinger CB, Edwards FA. Development of rat CA1 neurones in acute versus organotypic slices: role of experience in synaptic morphology and activity. J Physiol. 2003;550(Pt 1):135-47.
24. Stachniak TJ, Bourque CW. Visually guided whole cell patch clamp of mouse supraoptic nucleus neurons in cultured and acute conditions. Am J Physiol Regul Integr Comp Physiol. 2006;291(1):R68-76.
25. Bernardino L, Balosso S, Ravizza T, Marchi N, Ku G, Randle JC, et al. Inflammatory events in hippocampal slice cultures prime neuronal susceptibility to excitotoxic injury: a crucial role of P2X7 receptor-mediated IL-1beta release. J Neurochem. 2008;106(1):271-80.
26. Hailer NP, Jarhult JD, Nitsch R. Resting microglial cells in vitro: analysis of morphology and adhesion molecule expression in organotypic hippocampal slice cultures. Glia. 1996;18(4):319-31.
27. Kebir H, Carmant L, Fontaine F, Beland K, Bosoi CM, Sanon NT, et al. Humanized mouse model of Rasmussen's encephalitis supports the immune-mediated hypothesis. J Clin Invest. 2018;128(5):2000-9.
28. Inoue M, Williams KL, Gunn MD, Shinohara ML. NLRP3 inflammasome induces chemotactic immune cell migration to the CNS in experimental autoimmune encephalomyelitis. Proc Natl Acad Sci U S A. 2012;109(26):10480-5.
29. Dinarello CA. Overview of the IL-1 family in innate inflammation and acquired immunity. Immunol Rev. 2018;281(1):8-27.
30. He Y, Hara H, Nunez G. Mechanism and Regulation of NLRP3 Inflammasome Activation. Trends Biochem Sci. 2016;41(12):1012-21.
31. Fernandes-Alnemri T, Wu J, Yu JW, Datta P, Miller B, Jankowski W, et al. The pyroptosome: a supramolecular assembly of ASC dimers mediating inflammatory cell death via caspase-1 activation. Cell Death Differ. 2007;14(9):1590-604.

32. Faustin B, Lartigue L, Bruey JM, Luciano F, Sergienko E, Bailly-Maitre B, et al. Reconstituted NALP1 inflammasome reveals two-step mechanism of caspase-1 activation. Mol Cell. 2007;25(5):713-24.
33. Ficker E, Heinemann U. Slow and fast transient potassium currents in cultured rat hippocampal cells. J Physiol. 1992;445:431-55.
34. Thompson SH. Three pharmacologically distinct potassium channels in molluscan neurones. J Physiol. 1977;265(2):465-88.
35. Mitterdorfer J, Bean BP. Potassium currents during the action potential of hippocampal CA3 neurons. J Neurosci. 2002;22(23):10106-15.
36. Zou Z, Lu Y, Zha Y, Yang H. Endocannabinoid 2-Arachidonoylglycerol Suppresses LPS-Induced Inhibition of A-Type Potassium Channel Currents in Caudate Nucleus Neurons Through CB1 Receptor. J Mol Neurosci. 2016;59(4):493-503.
37. Storm JF. Temporal integration by a slowly inactivating K+ current in hippocampal neurons. Nature. 1988;336(6197):379-81.
38. Storm JF. Action potential repolarization and a fast after-hyperpolarization in rat hippocampal pyramidal cells. J Physiol. 1987;385:733-59.
39. Flores J, Noel A, Foveau B, Lynham J, Lecrux C, LeBlanc AC. Caspase-1 inhibition alleviates cognitive impairment and neuropathology in an Alzheimer's disease mouse model. Nat Commun. 2018;9(1):3916.
40. Zhang Y, Liu L, Liu YZ, Shen XL, Wu TY, Zhang T, et al. NLRP3 Inflammasome Mediates Chronic Mild Stress-Induced Depression in Mice via Neuroinflammation. Int J Neuropsychopharmacol. 2015;18(8).
41. McKenzie BA, Mamik MK, Saito LB, Boghozian R, Monaco MC, Major EO, et al. Caspase-1 inhibition prevents glial inflammasome activation and pyroptosis in models of multiple sclerosis. Proc Natl Acad Sci U S A. 2018;115(26):E6065-E74.
42. Riazi K, Galic MA, Pittman QJ. Contributions of peripheral inflammation to seizure susceptibility: cytokines and brain excitability. Epilepsy Res. 2010;89(1):34-42.
43. Freeman LC, Ting JP. The pathogenic role of the inflammasome in neurodegenerative diseases. J Neurochem. 2016;136 Suppl 1:29-38.
44. Mamik MK, Power C. Inflammasomes in neurological diseases: emerging pathogenic and therapeutic concepts. Brain. 2017;140(9):2273-85.
45. Semmler A, Okulla T, Sastre M, Dumitrescu-Ozimek L, Heneka MT. Systemic inflammation induces apoptosis with variable vulnerability of different brain regions. J Chem Neuroanat. 2005;30(2-3):144-57.
46. Ban E, Milon G, Prudhomme N, Fillion G, Haour F. Receptors for interleukin-1 (alpha and beta) in mouse brain: mapping and neuronal localization in hippocampus. Neuroscience. 1991;43(1):21-30.
47. Takao T, Tracey DE, Mitchell WM, De Souza EB. Interleukin-1 receptors in mouse brain: characterization and neuronal localization. Endocrinology. 1990;127(6):3070-8.

48. Ban EM. Interleukin-1 receptors in the brain: characterization by quantitative in situ autoradiography. Immunomethods. 1994;5(1):31-40.
49. Shrestha R, Millington O, Brewer J, Dev KK, Bushell TJ. Lymphocyte-mediated neuroprotection in in vitro models of excitotoxicity involves astrocytic activation and the inhibition of MAP kinase signalling pathways. Neuropharmacology. 2014;76 Pt A:184-93.
50. Araque A, Navarrete M. Glial cells in neuronal network function. Philos Trans R Soc Lond B Biol Sci. 2010;365(1551):2375-81.
51. Chong SA, Balosso S, Vandenplas C, Szczesny G, Hanon E, Claes K, et al. Intrinsic Inflammation Is a Potential Anti-Epileptogenic Target in the Organotypic Hippocampal Slice Model. Neurotherapeutics. 2018;15(2):470-88.
52. Basu S, Binder RJ, Suto R, Anderson KM, Srivastava PK. Necrotic but not apoptotic cell death releases heat shock proteins, which deliver a partial maturation signal to dendritic cells and activate the NF-kappa B pathway. Int Immunol. 2000;12(11):1539-46.
53. Swaroop S, Mahadevan A, Shankar SK, Adlakha YK, Basu A. HSP60 critically regulates endogenous IL-1beta production in activated microglia by stimulating NLRP3 inflammasome pathway. J Neuroinflammation. 2018;15(1):177.
54. Monaghan MM, Trimmer JS, Rhodes KJ. Experimental localization of Kv1 family voltage-gated K+ channel alpha and beta subunits in rat hippocampal formation. J Neurosci. 2001;21(16):5973-83.
55. Kole MH, Letzkus JJ, Stuart GJ. Axon initial segment Kv1 channels control axonal action potential waveform and synaptic efficacy. Neuron. 2007;55(4):633-47.
56. Hoffman DA, Magee JC, Colbert CM, Johnston D. K+ channel regulation of signal propagation in dendrites of hippocampal pyramidal neurons. Nature. 1997;387(6636):869-75.
57. Serodio P, Rudy B. Differential expression of Kv4 K+ channel subunits mediating subthreshold transient K+ (A-type) currents in rat brain. J Neurophysiol. 1998;79(2):1081-91.
58. de Rivero Vaccari JP, Lotocki G, Alonso OF, Bramlett HM, Dietrich WD, Keane RW. Therapeutic neutralization of the NLRP1 inflammasome reduces the innate immune response and improves histopathology after traumatic brain injury. J Cereb Blood Flow Metab. 2009;29(7):1251-61.
59. Abulafia DP, de Rivero Vaccari JP, Lozano JD, Lotocki G, Keane RW, Dietrich WD. Inhibition of the inflammasome complex reduces the inflammatory response after thromboembolic stroke in mice. J Cereb Blood Flow Metab. 2009;29(3):534-44.
60. Lei Z, Deng P, Li J, Xu ZC. Alterations of A-type potassium channels in hippocampal neurons after traumatic brain injury. J Neurotrauma. 2012;29(2):235-45.
61. Gruss M, Ettorre G, Stehr AJ, Henrich M, Hempelmann G, Scholz A. Moderate hypoxia influences excitability and blocks dendrotoxin sensitive K+ currents in rat primary sensory neurones. Mol Pain. 2006;2:12.
62. Pathak D, Guan D, Foehring RC. Roles of specific Kv channel types in repolarization of the action potential in genetically identified subclasses of pyramidal neurons in mouse neocortex. J Neurophysiol. 2016;115(5):2317-29.

63. Spigelman I, Zhang L, Carlen PL. Patch-clamp study of postnatal development of CA1 neurons in rat hippocampal slices: membrane excitability and K+ currents. J Neurophysiol. 1992;68(1):55-69.
64. Brown DA, Gahwiler BH, Griffith WH, Halliwell JV. Membrane currents in hippocampal neurons. Prog Brain Res. 1990;83:141-60.
65. Wannamaker W, Davies R, Namchuk M, Pollard J, Ford P, Ku G, et al. (S)-1-((S)-2-{[1-(4-amino-3-chloro-phenyl)-methanoyl]-amino}-3,3-dimethyl-butanoy l)-pyrrolidine-2-carboxylic acid ((2R,3S)-2-ethoxy-5-oxo-tetrahydro-furan-3-yl)-amide (VX-765), an orally available selective interleukin (IL)-converting enzyme/caspase-1 inhibitor, exhibits potent anti-inflammatory activities by inhibiting the release of IL-1beta and IL-18. J Pharmacol Exp Ther. 2007;321(2):509-16.
66. Ravizza T, Lucas SM, Balosso S, Bernardino L, Ku G, Noe F, et al. Inactivation of caspase-1 in rodent brain: a novel anticonvulsive strategy. Epilepsia. 2006;47(7):1160-8.
67. Tan CC, Zhang JG, Tan MS, Chen H, Meng DW, Jiang T, et al. NLRP1 inflammasome is activated in patients with medial temporal lobe epilepsy and contributes to neuronal pyroptosis in amygdala kindling-induced rat model. J Neuroinflammation. 2015;12:18.
68. Meng XF, Tan L, Tan MS, Jiang T, Tan CC, Li MM, et al. Inhibition of the NLRP3 inflammasome provides neuroprotection in rats following amygdala kindling-induced status epilepticus. J Neuroinflammation. 2014;11:212.
69. Maroso M, Balosso S, Ravizza T, Iori V, Wright CI, French J, et al. Interleukin-1beta biosynthesis inhibition reduces acute seizures and drug resistant chronic epileptic activity in mice. Neurotherapeutics. 2011;8(2):304-15.
70. Gimsa U, Peter SV, Lehmann K, Bechmann I, Nitsch R. Axonal damage induced by invading T cells in organotypic central nervous system tissue in vitro: involvement of microglial cells. Brain Pathol. 2000;10(3):365-77.
71. Nitsch R, Pohl EE, Smorodchenko A, Infante-Duarte C, Aktas O, Zipp F. Direct impact of T cells on neurons revealed by two-photon microscopy in living brain tissue. J Neurosci. 2004;24(10):2458-64.
72. Mori F, Nistico R, Mandolesi G, Piccinin S, Mango D, Kusayanagi H, et al. Interleukin-1beta promotes long-term potentiation in patients with multiple sclerosis. Neuromolecular Med. 2014;16(1):38-51.
73. Eisenberg SP, Evans RJ, Arend WP, Verderber E, Brewer MT, Hannum CH, et al. Primary structure and functional expression from complementary DNA of a human interleukin-1 receptor antagonist. Nature. 1990;343(6256):341-6.

Figures

FIG. 1

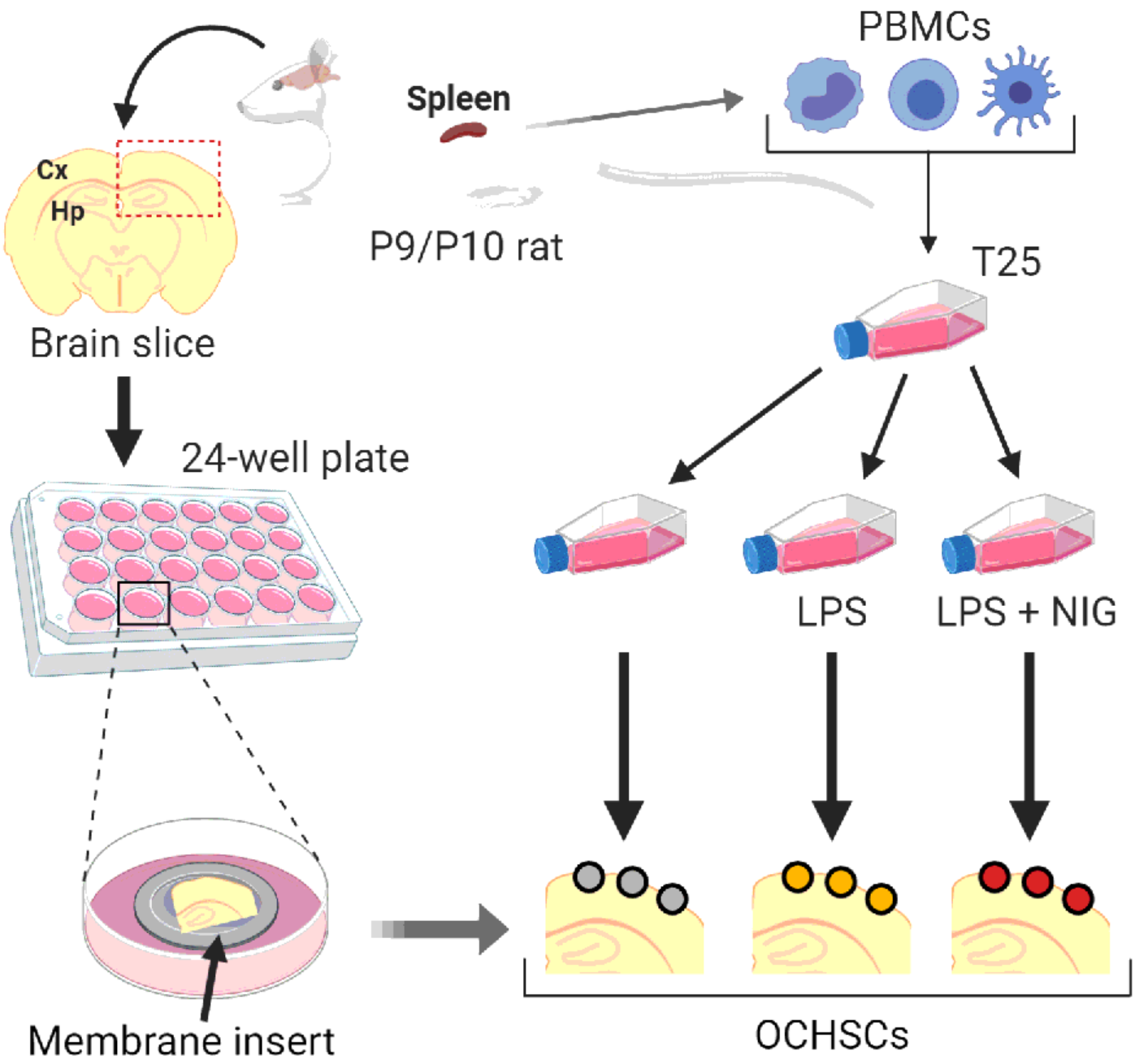

Figure 1

Establishment of the PBMC-OCHSC co-culture system. Schematic illustration showing the experimental design of the in vitro model. Brain slices were prepared from of P9/P10 Sprague-Dawley male rats, where slices were trimmed to only contain the cortex (Cx) and the hippocampus (Hp) from each hemisphere. To obtain OCHSCs, slices were individually placed on top a membrane inset and grown in 24-well plates supplied with culture media. PBMCs were simultaneously extracted from the spleen of the same rat and cultured in T25 flasks. At 3 DIV, PBMCs were divided into three different flasks. At 6 DIV, the first flask was

left untreated (grey circles), the second was treated with LPS for 3-3.5 hours (yellow circles), and the third was treated with LPS for 3-3.5 hours followed by nigericin (NIG) for 2.5-3 hours (red circles). After washing out the drugs, PBMCs from each flask were concentrated, and ~3.0 × 104 cells were added on top of the cortex of each OCHSC.

FIG. 1

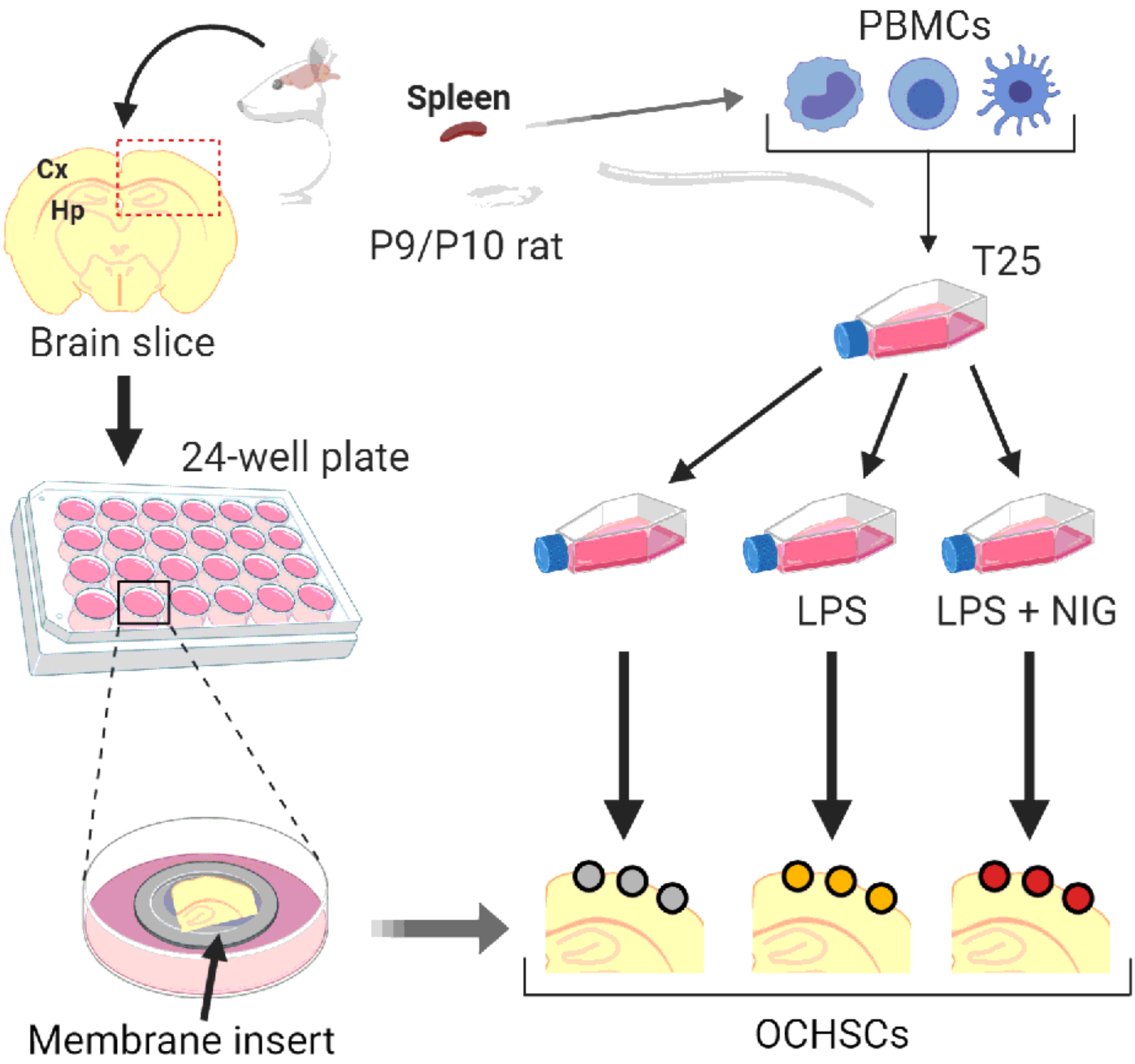

Figure 1

Establishment of the PBMC-OCHSC co-culture system. Schematic illustration showing the experimental design of the in vitro model. Brain slices were prepared from of P9/P10 Sprague-Dawley male rats, where

slices were trimmed to only contain the cortex (Cx) and the hippocampus (Hp) from each hemisphere. To obtain OCHSCs, slices were individually placed on top a membrane inset and grown in 24-well plates supplied with culture media. PBMCs were simultaneously extracted from the spleen of the same rat and cultured in T25 flasks. At 3 DIV, PBMCs were divided into three different flasks. At 6 DIV, the first flask was left untreated (grey circles), the second was treated with LPS for 3-3.5 hours (yellow circles), and the third was treated with LPS for 3-3.5 hours followed by nigericin (NIG) for 2.5-3 hours (red circles). After washing out the drugs, PBMCs from each flask were concentrated, and ~3.0 × 104 cells were added on top of the cortex of each OCHSC.

FIG. 2

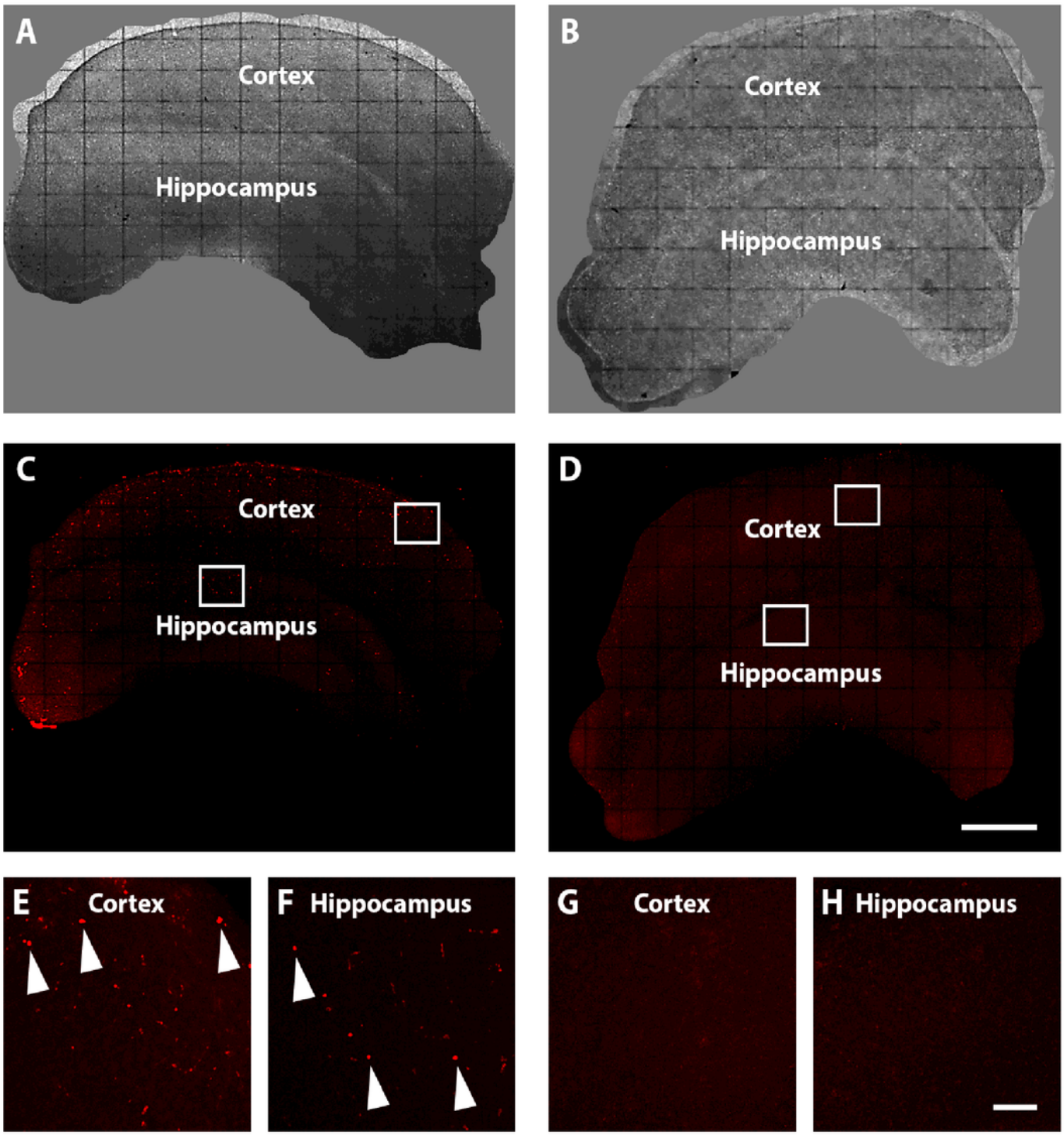

Figure 2

The OCHSC membrane insert acts as a barrier by preventing PBMCs infiltration. (A-D) Mosaic images stitched to show OCHSCs co-cultured with CFSE+ PBMCs added on top of the cortex (A, C), and OCSHCs co-cultured with CFSE+ PBMCs added to the media where OCHSCs and PBMCs are separated by the membrane insert (B, D), viewed in bright field (A, B) and under fluorescent light (C, D). (E-H) Insets of white boxes in C and D, showing the cortex (E, G) and the hippocampus (F, H) of OCHSCs co-cultured directly

with CFSE+ PBMCs (E, F) and OCHSCs co-cultured separately from media-incubated CFSE+ PBMCs (G, H). White arrowheads in E and F mark CFSE+ PBMCs respectively adhering to cortical and hippocampal tissue in OCHSCs. Scale bars, 1 mm (A-D), 100 µm (E-H).

FIG. 2

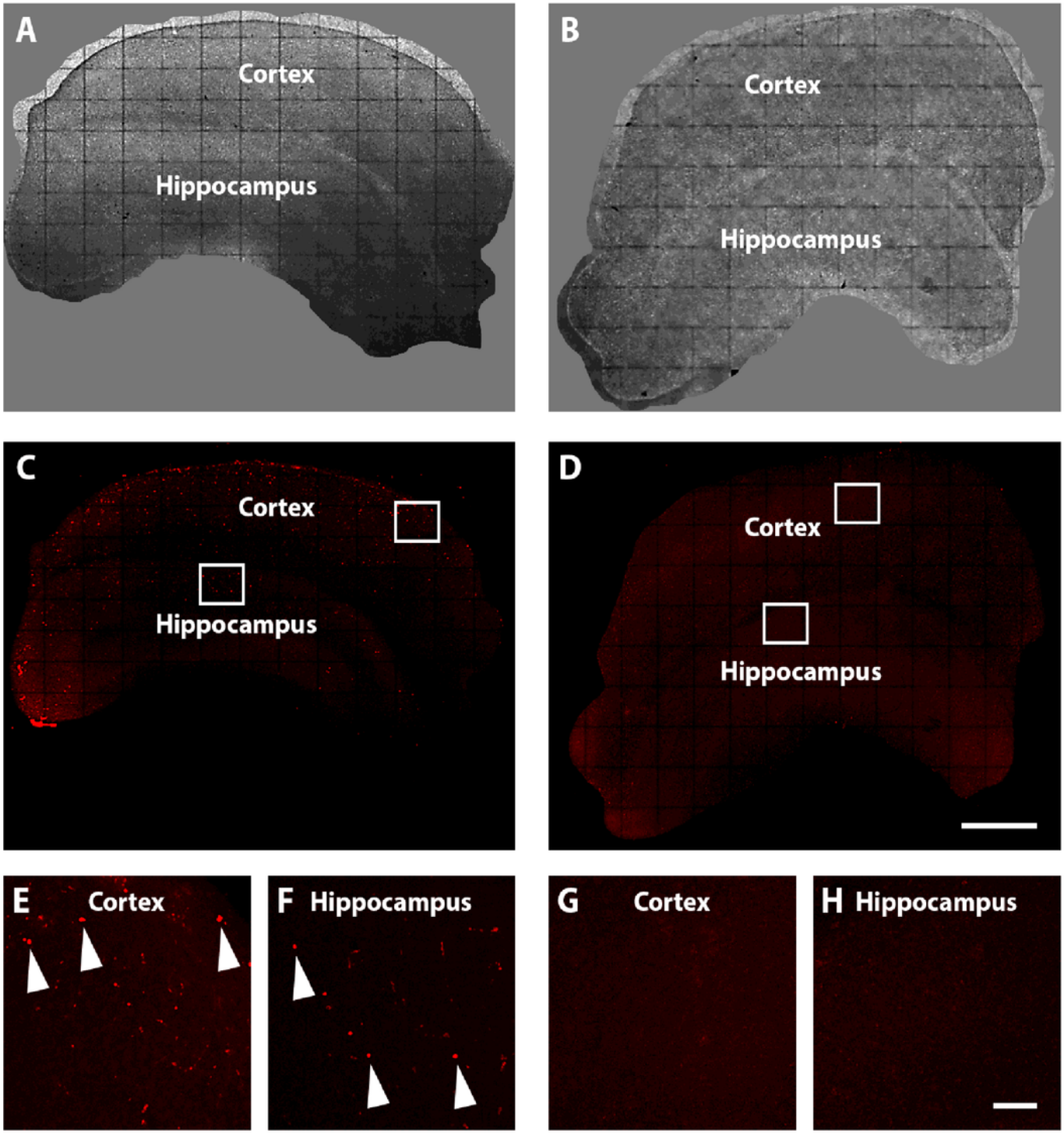

Figure 2

The OCHSC membrane insert acts as a barrier by preventing PBMCs infiltration. (A-D) Mosaic images stitched to show OCHSCs co-cultured with CFSE+ PBMCs added on top of the cortex (A, C), and OCSHCs

co-cultured with CFSE+ PBMCs added to the media where OCHSCs and PBMCs are separated by the membrane insert (B, D), viewed in bright field (A, B) and under fluorescent light (C, D). (E-H) Insets of white boxes in C and D, showing the cortex (E, G) and the hippocampus (F, H) of OCHSCs co-cultured directly with CFSE+ PBMCs (E, F) and OCHSCs co-cultured separately from media-incubated CFSE+ PBMCs (G, H). White arrowheads in E and F mark CFSE+ PBMCs respectively adhering to cortical and hippocampal tissue in OCHSCs. Scale bars, 1 mm (A-D), 100 μm (E-H).

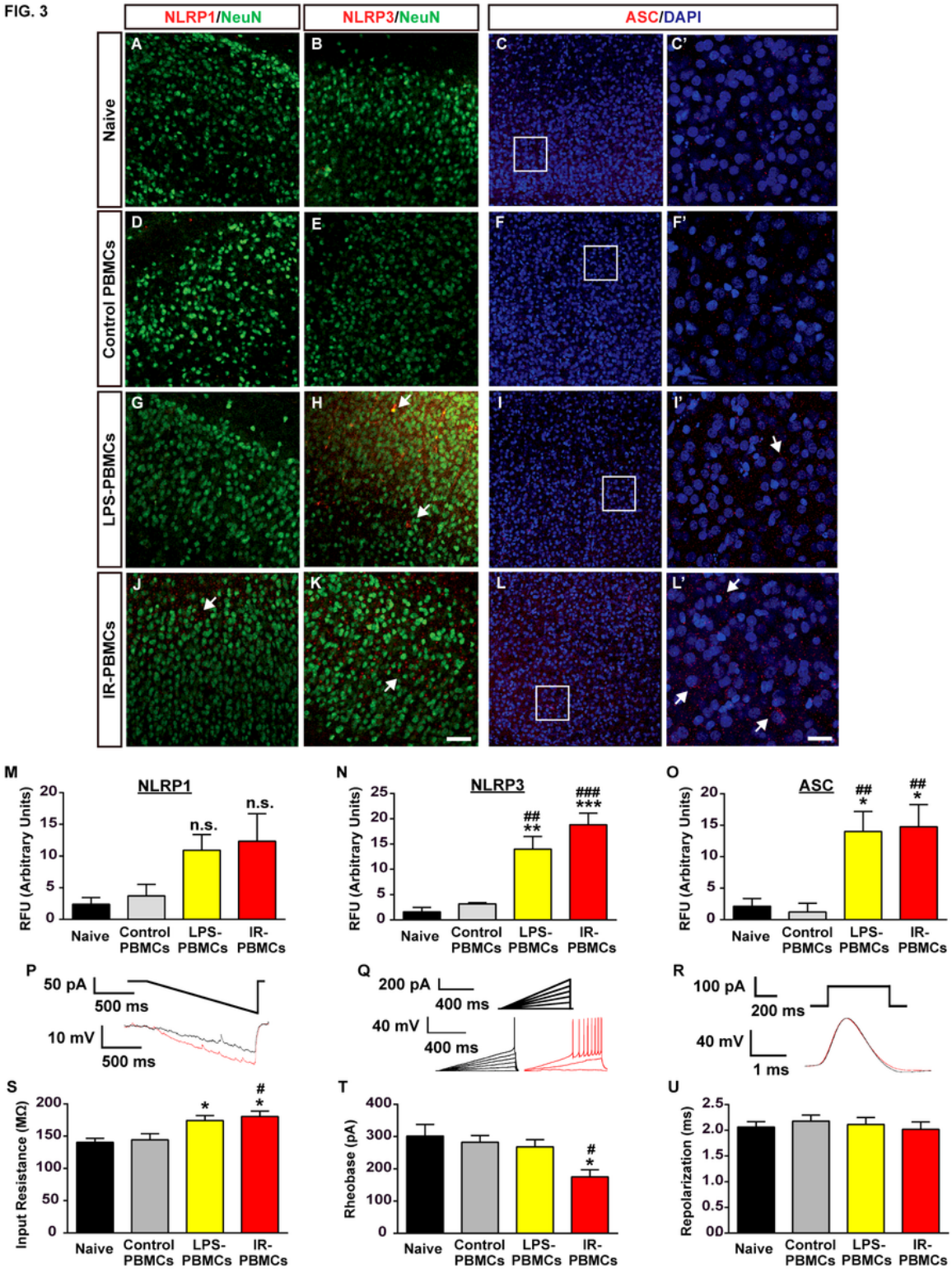

Figure 3

Pro-inflammatory PBMCs induce neuroinflammation and hyperexcitability in the cortex. (A-L´) Immunohistochemical double-staining of NLRP1/NeuN (A, D, G, J), NLRP3/NeuN (B, E, H, K) and ASC/DAPI (C, C´, F, F´, I, I´, L, L´) in cortical tissue of naive OCHSCs (A-C´) compared to OCHSCs co-cultured with control PBMCs (D-F´), LPS-PBMCs (G-I´) and IR-PBMCs (J-L´). C´, F´, I´, L´ are magnified images of white boxes in C, F, I, L, respectively. White arrows denote ectopic expression of NLRP1 in J, NLRP3 in H, K, and ASC in I´, L´. (M, N, O) Mean semi-quantitative immunofluorescence of NLRP1 (M), NLRP3 (N), and ASC (O) in cortical tissue of naive OCHSCs (NLRP1: n = 5; NLRP3: n = 4; ASC: n = 5) compared to OCHSCs co-cultured with control PBMCs (NLRP1: n = 4; NLRP3: n = 5; ASC: n = 5), LPS-PBMCs (NLRP1: n = 5; NLRP3: n = 6; ASC: n = 5) and IR-PBMCs (NLRP1: n = 5; NLRP3: n = 4; ASC: n = 4). (P, Q, R) Representative input traces (top) and cell output (bottom) recorded in current clamp in response to: a hyperpolarizing 100 pA ramp (P), depolarizing 100 pA ramps in 100 pA increments (Q), and a depolarizing 100 pA step current (R), in cortical pyramidal neurons from naive OCHSCs (black) and OCHSCs co-cultured with IR-PBMCs (red). (S, T, U) Mean input resistance (S), rheobase (T), and repolarization time (U) in cortical pyramidal neurons of naive OCHSCs (n = 11) along with OCHSCs co-cultured with control PBMCs (n = 11), LPS-PBMCs (n = 10) and IR-PBMCs (n = 10). Error bars represent mean ± SEM; *p < 0.05, **p < 0.01, ***p < 0.001 compared to naive, #p < 0.05, ##p < 0.01, ###p < 0.001 compared to control PBMCs by Bonferroni test. Scale bars, 100 μm (A-L), 50 μm (C´-L´).

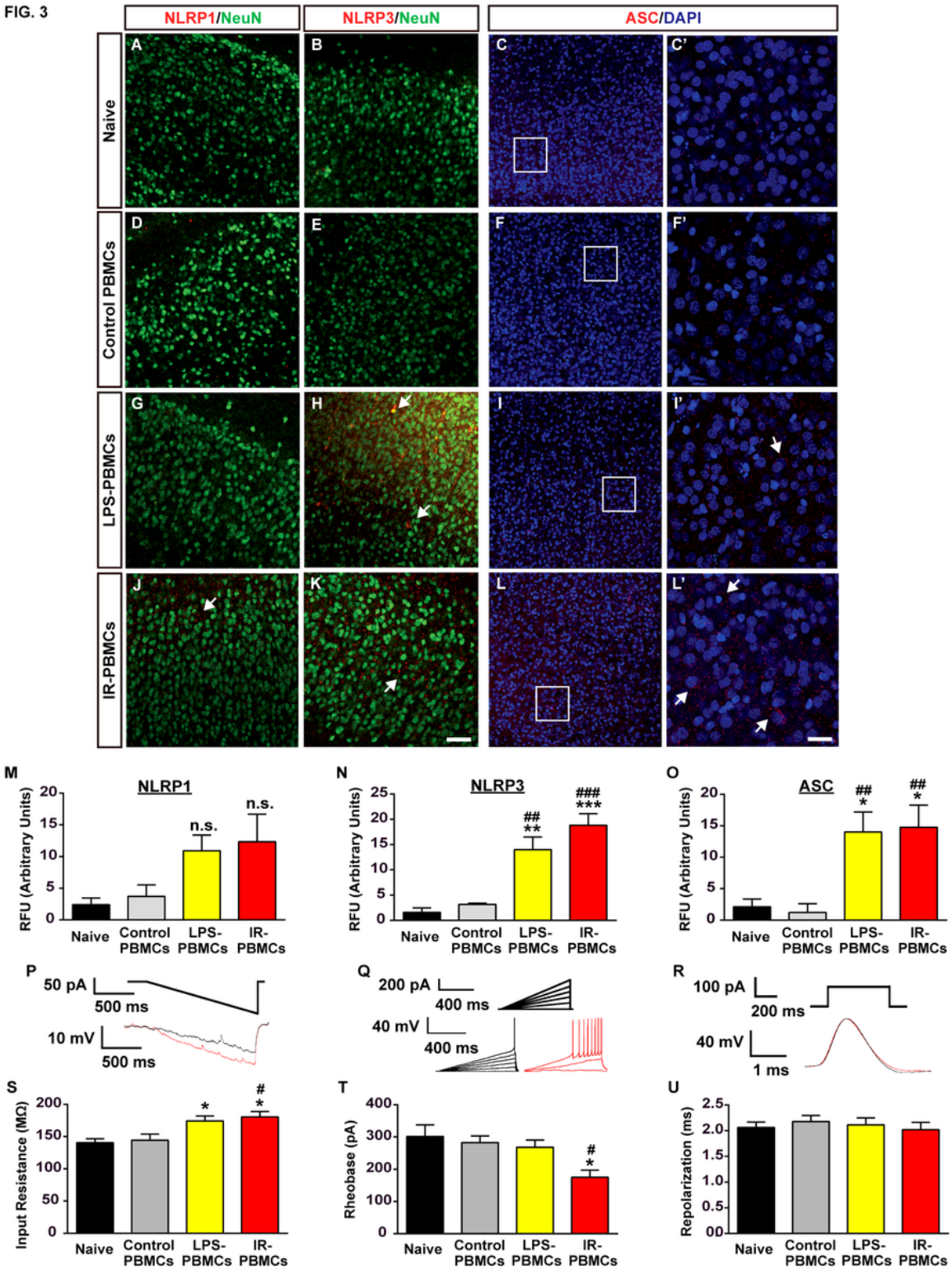

Figure 3

Pro-inflammatory PBMCs induce neuroinflammation and hyperexcitability in the cortex. (A-L´) Immunohistochemical double-staining of NLRP1/NeuN (A, D, G, J), NLRP3/NeuN (B, E, H, K) and ASC/DAPI (C, C´, F, F´, I, I´, L, L´) in cortical tissue of naive OCHSCs (A-C´) compared to OCHSCs co-cultured with control PBMCs (D-F´), LPS-PBMCs (G-I´) and IR-PBMCs (J-L´). C´, F´, I´, L´ are magnified images of white boxes in C, F, I, L, respectively. White arrows denote ectopic expression of NLRP1 in J,

NLRP3 in H, K, and ASC in I´, L´. (M, N, O) Mean semi-quantitative immunofluorescence of NLRP1 (M), NLRP3 (N), and ASC (O) in cortical tissue of naive OCHSCs (NLRP1: n = 5; NLRP3: n = 4; ASC: n = 5) compared to OCHSCs co-cultured with control PBMCs (NLRP1: n = 4; NLRP3: n = 5; ASC: n = 5), LPS-PBMCs (NLRP1: n = 5; NLRP3: n = 6; ASC: n = 5) and IR-PBMCs (NLRP1: n = 5; NLRP3: n = 4; ASC: n = 4). (P, Q, R) Representative input traces (top) and cell output (bottom) recorded in current clamp in response to: a hyperpolarizing 100 pA ramp (P), depolarizing 100 pA ramps in 100 pA increments (Q), and a depolarizing 100 pA step current (R), in cortical pyramidal neurons from naive OCHSCs (black) and OCHSCs co-cultured with IR-PBMCs (red). (S, T, U) Mean input resistance (S), rheobase (T), and repolarization time (U) in cortical pyramidal neurons of naive OCHSCs (n = 11) along with OCHSCs co-cultured with control PBMCs (n = 11), LPS-PBMCs (n = 10) and IR-PBMCs (n = 10). Error bars represent mean ± SEM; *p < 0.05, **p < 0.01, ***p < 0.001 compared to naive, #p < 0.05, ##p < 0.01, ###p < 0.001 compared to control PBMCs by Bonferroni test. Scale bars, 100 µm (A-L), 50 µm (C´-L´).

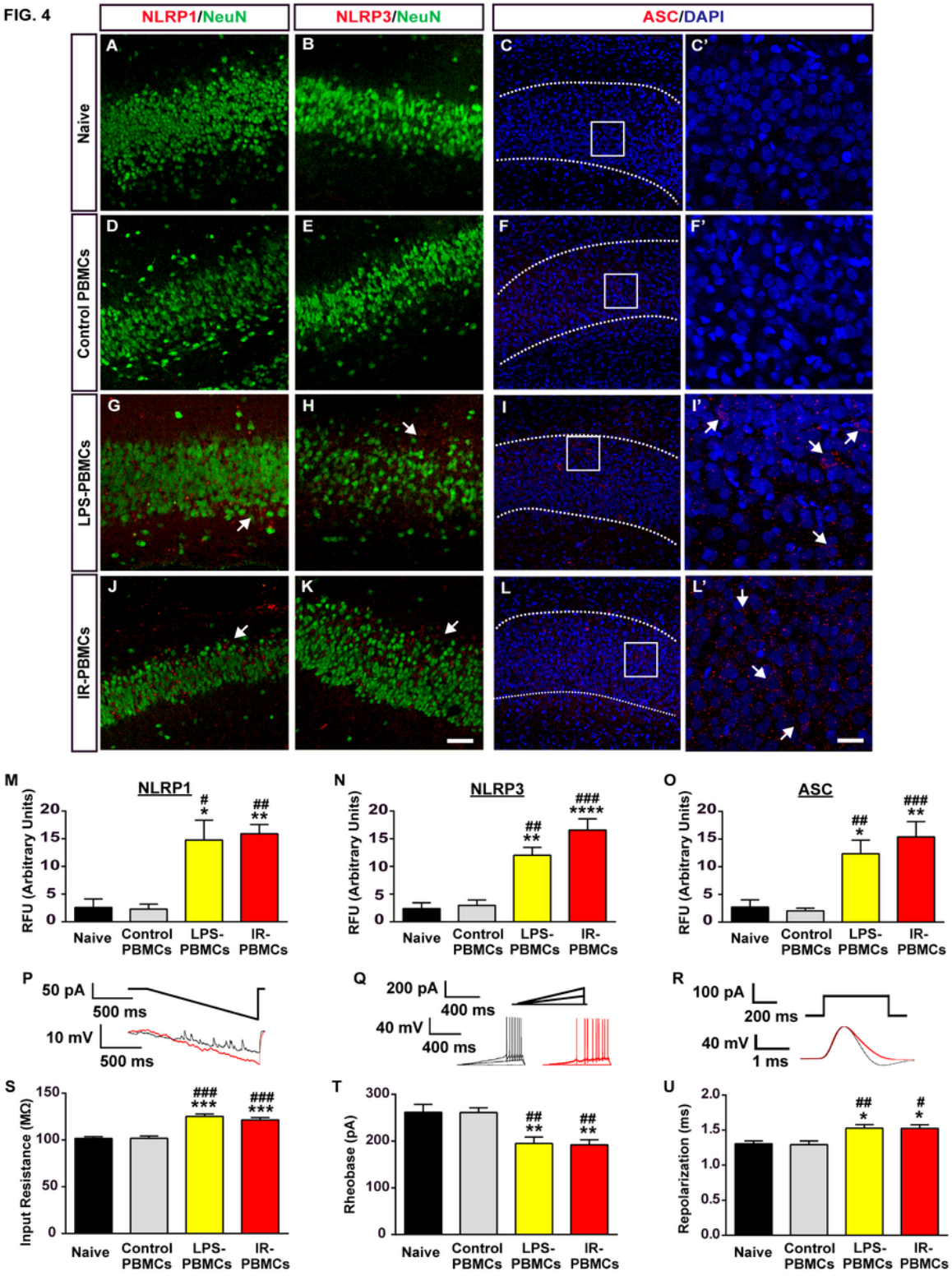

Figure 4

Priming inflammation in PBMCs is sufficient to induce neuroinflammation and hyperexcitability in the hippocampus. (A-L´) Immunohistochemical double-staining of NLRP1/NeuN (A, D, G, J), NLRP3/NeuN (B, E, H, K) and ASC/DAPI (C, C´, F, F´, I, I´, L, L´) in hippocampal tissue of naive OCHSCs (A-C´) compared to OCHSCs co-cultured with control PBMCs (D-F´), LPS-PBMCs (G-I´) and IR-PBMCs (J-L´). C´, F´, I´, L´ are magnified images of white boxes in C, F, I, L, respectively. White arrows denote ectopic expression of

NLRP1 in G, J, NLRP3 in H, K, and ASC in I´, L´. (M, N, O) Mean semi-quantitative immunofluorescence of NLRP1 (M), NLRP3 (N), and ASC (O) in hippocampal tissue of naive OCHSCs (NLRP1: n = 4; NLRP3: n = 4; ASC: n = 4) compared to OCHSCs co-cultured with control PBMCs (NLRP1: n = 4; NLRP3: n = 4; ASC: n = 5), LPS-PBMCs (NLRP1: n = 5; NLRP3: n = 6; ASC: n = 4) and IR-PBMCs (NLRP1: n = 5; NLRP3: n = 5; ASC: n = 4). (P, Q, R) Representative input traces (top) and cell output (bottom) recorded in current clamp in response to: a hyperpolarizing 100 pA ramp (P), depolarizing 100 pA ramps in 100 pA increments (Q), and a depolarizing 100 pA step current (R), in hippocampal pyramidal neurons from naive OCHSCs (black) and OCHSCs co-cultured with IR-PBMCs (red). (S, T, U) Mean input resistance (S), rheobase (T), and repolarization time (U) in hippocampal pyramidal neurons of naive OCHSCs (n = 23) together with OCHSCs co-cultured with control PBMCs (n = 21), LPS-PBMCs (n = 19) and IR-PBMCs (n = 20). Error bars represent mean ± SEM; *p < 0.05, **p < 0.01, ***p < 0.001, ****p < 0.0001 compared to naive, #p < 0.05, ##p < 0.01, ###p < 0.001 compared to control PBMCs by Bonferroni test. Scale bars, 100 µm (A-L), 50 µm (C´-L´).

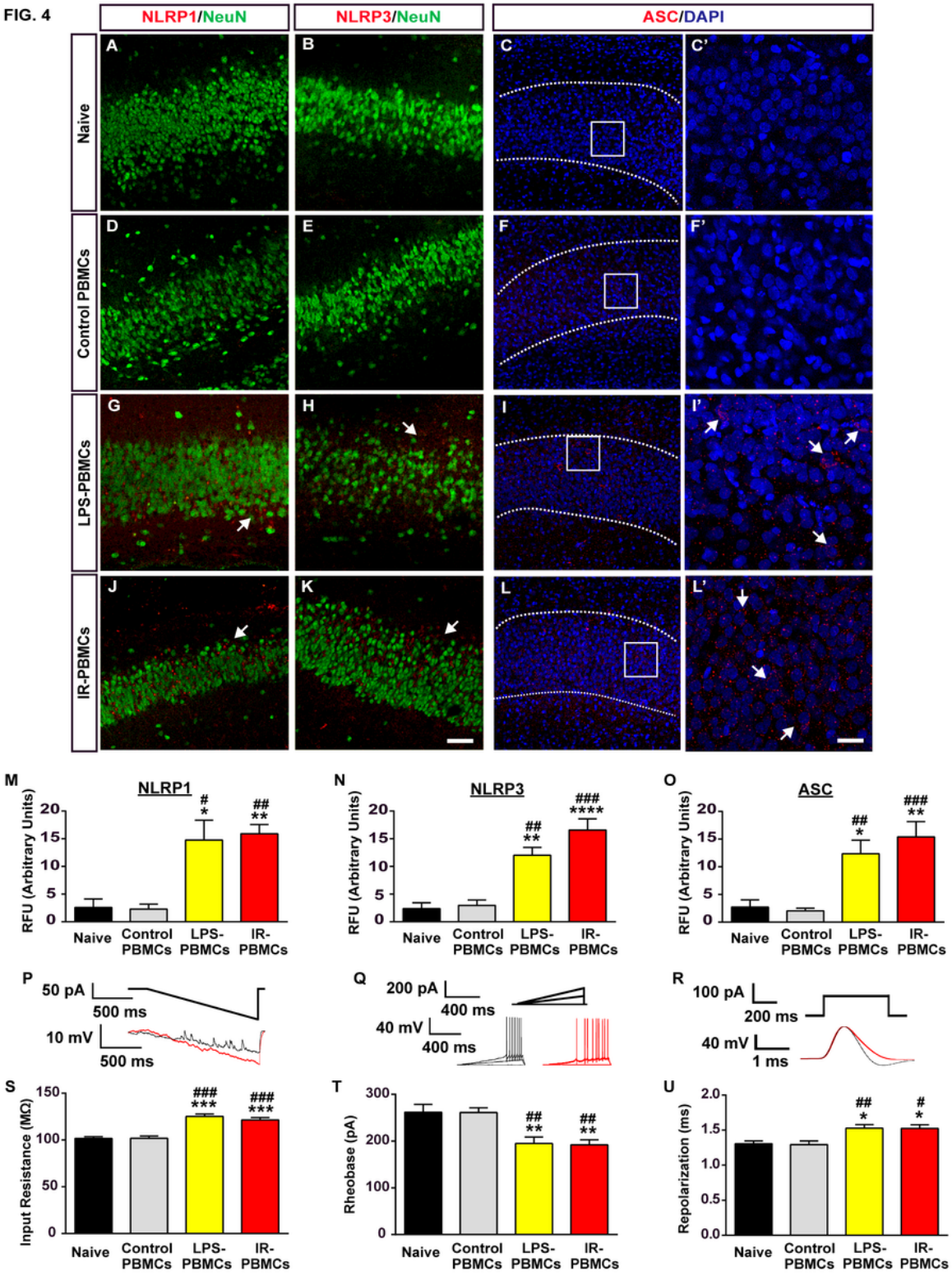

Figure 4

Priming inflammation in PBMCs is sufficient to induce neuroinflammation and hyperexcitability in the hippocampus. (A-L´) Immunohistochemical double-staining of NLRP1/NeuN (A, D, G, J), NLRP3/NeuN (B, E, H, K) and ASC/DAPI (C, C´, F, F´, I, I´, L, L´) in hippocampal tissue of naive OCHSCs (A-C´) compared to OCHSCs co-cultured with control PBMCs (D-F´), LPS-PBMCs (G-I´) and IR-PBMCs (J-L´). C´, F´, I´, L´ are magnified images of white boxes in C, F, I, L, respectively. White arrows denote ectopic expression of

NLRP1 in G, J, NLRP3 in H, K, and ASC in I´, L´. (M, N, O) Mean semi-quantitative immunofluorescence of NLRP1 (M), NLRP3 (N), and ASC (O) in hippocampal tissue of naive OCHSCs (NLRP1: n = 4; NLRP3: n = 4; ASC: n = 4) compared to OCHSCs co-cultured with control PBMCs (NLRP1: n = 4; NLRP3: n = 4; ASC: n = 5), LPS-PBMCs (NLRP1: n = 5; NLRP3: n = 6; ASC: n = 4) and IR-PBMCs (NLRP1: n = 5; NLRP3: n = 5; ASC: n = 4). (P, Q, R) Representative input traces (top) and cell output (bottom) recorded in current clamp in response to: a hyperpolarizing 100 pA ramp (P), depolarizing 100 pA ramps in 100 pA increments (Q), and a depolarizing 100 pA step current (R), in hippocampal pyramidal neurons from naive OCHSCs (black) and OCHSCs co-cultured with IR-PBMCs (red). (S, T, U) Mean input resistance (S), rheobase (T), and repolarization time (U) in hippocampal pyramidal neurons of naive OCHSCs (n = 23) together with OCHSCs co-cultured with control PBMCs (n = 21), LPS-PBMCs (n = 19) and IR-PBMCs (n = 20). Error bars represent mean ± SEM; *p < 0.05, **p < 0.01, ***p < 0.001, ****p < 0.0001 compared to naive, #p < 0.05, ##p < 0.01, ###p < 0.001 compared to control PBMCs by Bonferroni test. Scale bars, 100 µm (A-L), 50 µm (C´-L´).

FIG. 5

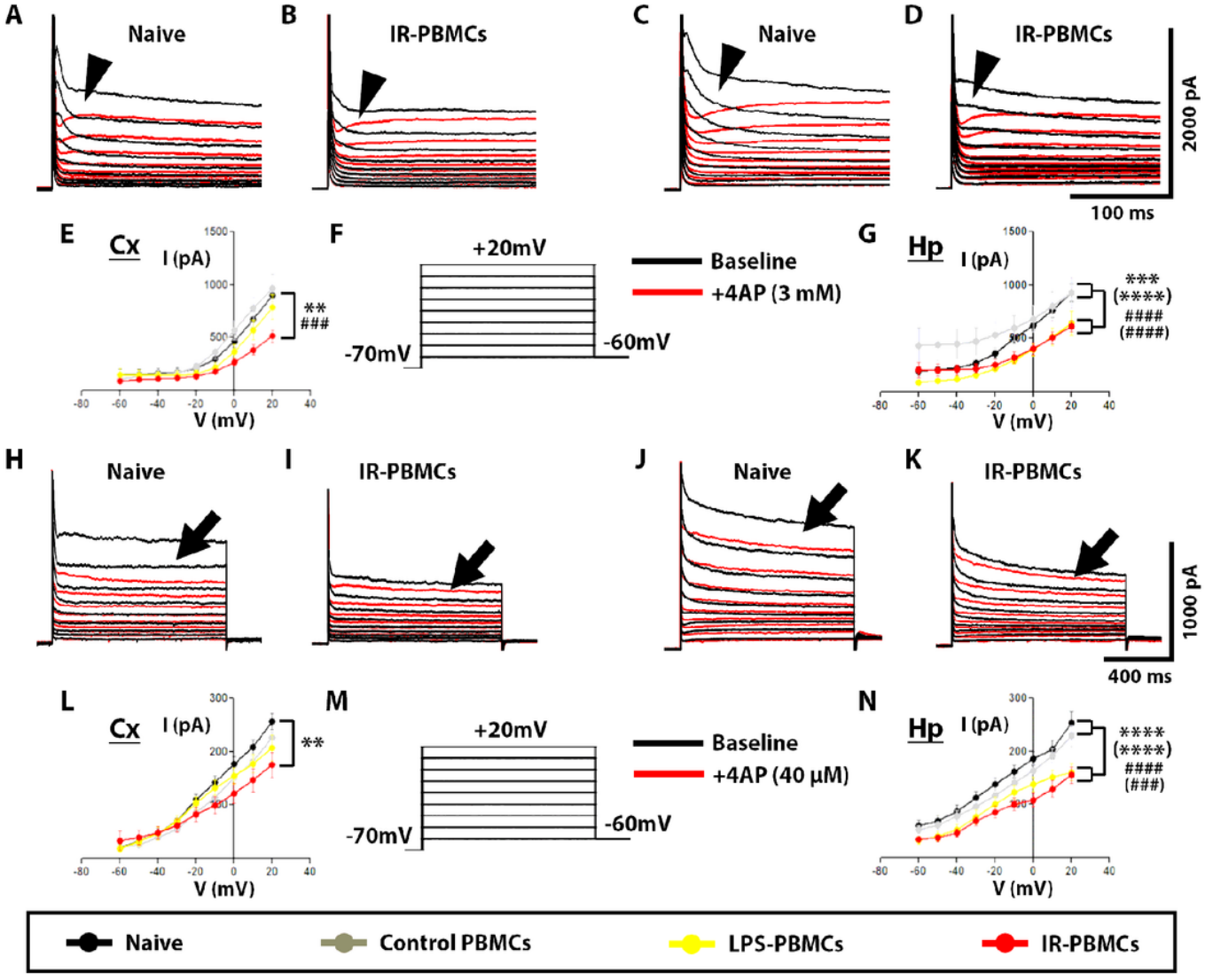

Figure 5

Transduction of peripheral inflammation impairs 4-AP sensitive currents in cortical and hippocampal neurons. (A-D, H-K) Representative IA (A-D) and ID (H-K) output traces, calculated by subtracting cell response following 3 mM (A-D) and 40 μM (H-K) 4-AP application (red traces) from baseline conditions (black traces) in cortical (A, B, H, I) and hippocampal (C, D, J, K) pyramidal neurons from naive OCHSCs (A, C, H, J) and OCHSCs co-cultured with IR-PBMCs (B, D, I, K). (E, G, L, N) I-V graphs of IA (E, G) and ID (L, N) in cortical (Cx) (E, L) and hippocampal (Hp) (G, N) pyramidal neurons of naive OCHSCs (back) (cortex: IA, n = 6; ID, n = 9; hippocampus: IA, n = 7; ID, n = 11) compared to OCHSCs co-cultured with control PBMCs (grey) (cortex: IA, n = 6; ID, n = 8; hippocampus: IA, n = 6; ID, n = 12), LPS-PBMCs (yellow) (cortex: IA, n = 6; ID, n = 9; hippocampus: IA, n = 6; ID, n = 12) and IR-PBMCs (red) (cortex: IA, n = 6; ID, n = 6; hippocampus: IA, n = 9; ID, n = 11). (F, M) Voltage input of +10 mV incremental depolarizing steps between −60 and +20 mV while constantly holding the cells at -70 mV. Black arrowheads in A, B, C, D denote the difference between baseline and 3mM 4-AP traces, i.e. IA, at maximum voltage input (+20 mV); black arrows in H, I, J, K denote the difference between baseline and 40 μM 4-AP traces, i.e. ID, at +20 mV. Error bars represent mean ± SEM; **$p < 0.01$, ***$p < 0.001$, ****$p < 0.0001$ IR-PBMCs compared to naive, ###$p < 0.001$, ####$p < 0.0001$ IR-PBMCs compared to control PBMCs, (****)$p < 0.0001$ LPS-PBMCs compared to naive, (###)$p < 0.001$, (####)$p < 0.0001$ LPS-PBMCs compared to control PBMCs by Bonferroni test.

FIG. 5

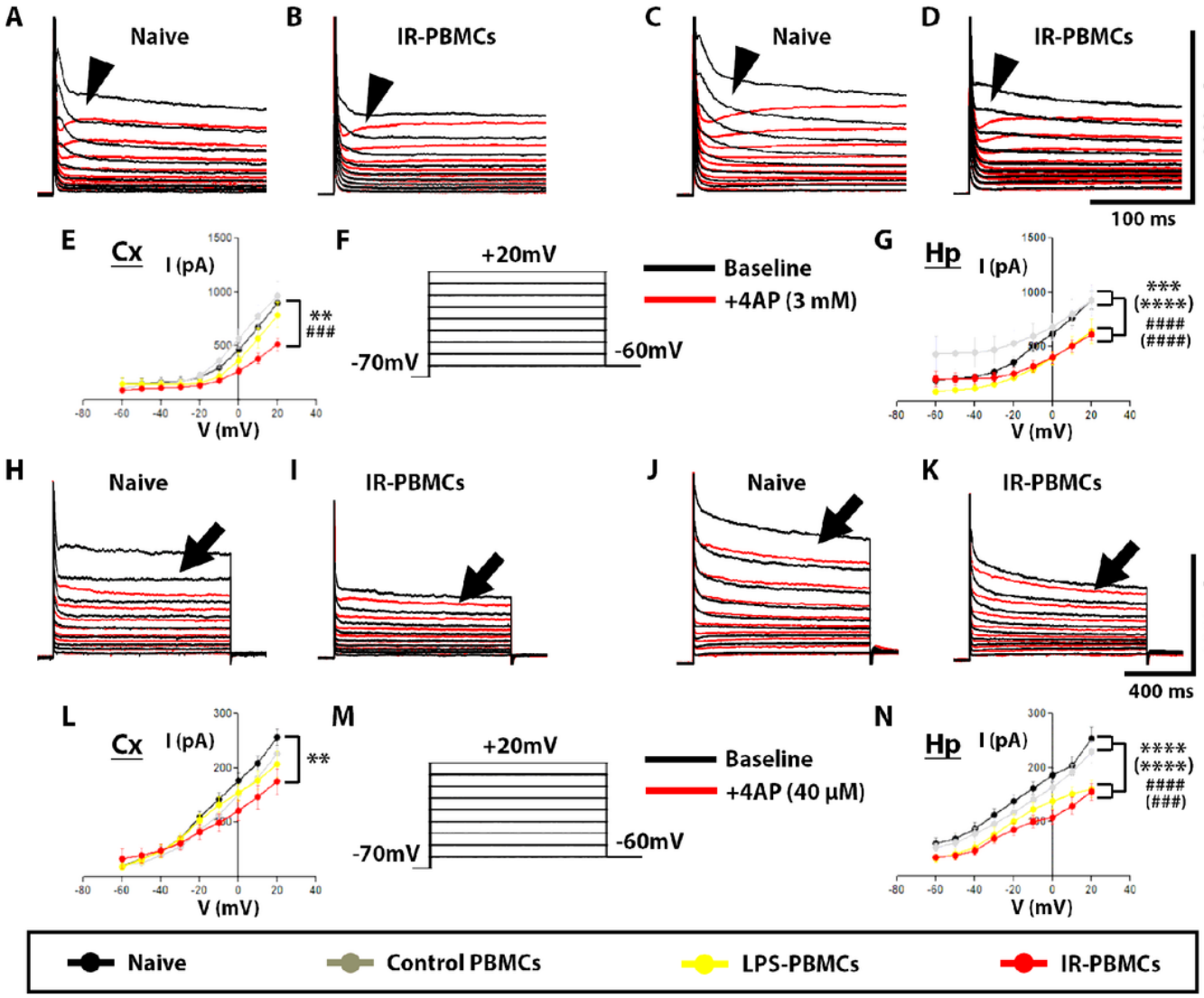

Figure 5

Transduction of peripheral inflammation impairs 4-AP sensitive currents in cortical and hippocampal neurons. (A-D, H-K) Representative IA (A-D) and ID (H-K) output traces, calculated by subtracting cell response following 3 mM (A-D) and 40 µM (H-K) 4-AP application (red traces) from baseline conditions (black traces) in cortical (A, B, H, I) and hippocampal (C, D, J, K) pyramidal neurons from naive OCHSCs (A, C, H, J) and OCHSCs co-cultured with IR-PBMCs (B, D, I, K). (E, G, L, N) I-V graphs of IA (E, G) and ID (L, N) in cortical (Cx) (E, L) and hippocampal (Hp) (G, N) pyramidal neurons of naive OCHSCs (back) (cortex: IA, n = 6; ID, n = 9; hippocampus: IA, n = 7; ID, n = 11) compared to OCHSCs co-cultured with control PBMCs (grey) (cortex: IA, n = 6; ID, n = 8; hippocampus: IA, n = 6; ID, n = 12), LPS-PBMCs (yellow) (cortex: IA, n = 6; ID, n = 9; hippocampus: IA, n = 6; ID, n = 12) and IR-PBMCs (red) (cortex: IA, n = 6; ID, n = 6; hippocampus: IA, n = 9; ID, n = 11). (F, M) Voltage input of +10 mV incremental depolarizing steps between −60 and +20 mV while constantly holding the cells at -70 mV. Black arrowheads in A, B, C, D denote the difference between baseline and 3mM 4-AP traces, i.e. IA, at maximum voltage input (+20 mV); black arrows in H, I, J, K denote the difference between baseline and 40 µM 4-AP traces, i.e. ID, at +20 mV.

Error bars represent mean ± SEM; **p < 0.01, ***p < 0.001, ****p < 0.0001 IR-PBMCs compared to naive, ###p < 0.001, ####p < 0.0001 IR-PBMCs compared to control PBMCs, (****)p < 0.0001 LPS-PBMCs compared to naive, (###)p < 0.001, (####)p < 0.0001 LPS-PBMCs compared to control PBMCs by Bonferroni test.

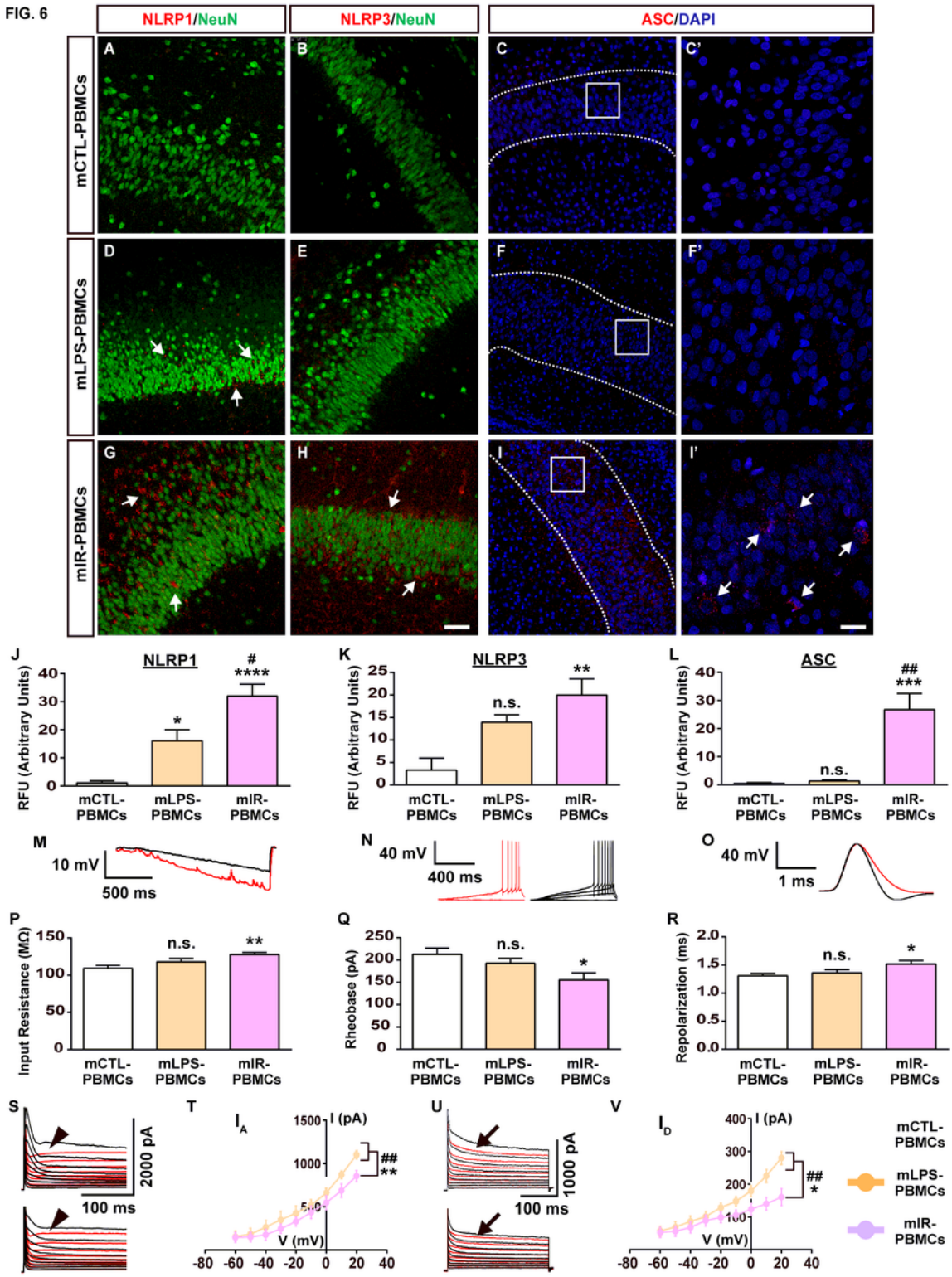

Figure 6

Cell-cell contact between LPS-PBMCs and OCHSCs is necessary for transduction of peripheral inflammation. (A-I´) Immunohistochemistry images of NLRP1/NeuN (A, D, G), NLRP3/NeuN (B, E, H) and ASC/DAPI (C, C´, F, F´, I, I´) in the hippocampus of mCTL-PBMC-OCHSCs (A-C´), mLPS-PBMC-OCHSCs (D-F´) and mIR-PBMC-OCHSCs (G-I´). C´, F´, I´ are magnified images of white boxes in C, F, I, respectively. White arrows in D, G, H, I´ mark inflammasome marker upregulation. (J) NLRP1, (K) NLRP3 and (L) ASC mean semi-quantitative immunofluorescence in hippocampal tissue of mCTL-PBMC-OCHSCs (NLRP1: n = 5; NLRP3: n = 4; ASC: n = 4), mLPS-PBMC-OCHSCs (NLRP1: n = 5; NLRP3: n = 5; ASC: n = 4) and mIR-PBMC-OCHSCs (NLRP1: n = 5; NLRP3: n = 5; ASC: n = 4). (M) input resistance, (N) rheobase and (O) repolarization sample outputs from mCTL-PBMC-OCHSCs (black) and mIR-PBMC-OCHSCs (red) hippocampal neurons, using Figures 4P, 4Q, 4R input protocols, respectively. (P) input resistance, (Q) rheobase and (R) repolarization time bar graphs of mCTL-PBMC-OCHSCs (n = 11), mLPS-PBMC-OCHSCs (n = 11) and mIR-PBMC-OCHSCs (n = 10) hippocampal neurons. (S) IA and (U) ID sample outputs from mCTL-PBMC-OCHSCs (top) and mIR-PBMC-OCHSCs (bottom), using Figures 5F and 5M input protocols (black traces: baseline, red traces: +4-AP; see Figure 5 legend). Black arrowheads and black arrows respectively denote maximum IA and ID in S and U (see Figure 5 legend). (T) IA and (V) ID I-V graphs of hippocampal neurons from mCTL-PBMC-OCHSCs (light grey) (IA, n = 6; ID, n = 8), LPS-PBMC-OCHSCs (orange) (IA, n = 5; ID, n = 8) and IR-PBMC-OCHSCs (pink) (IA, n = 5; ID, n = 7). Error bars represent mean ± SEM; n.s. denotes not significant, *p < 0.05, **p < 0.01, ***p < 0.001, ****p < 0.0001 compared to mCTL-PBMC-OCHSCs; #p < 0.05, ##p < 0.01 compared to mLPS-PBMC-OCHSCs by Bonferroni test. Scale bars, 100 μm (A-I), 50 μm (C´-I´).

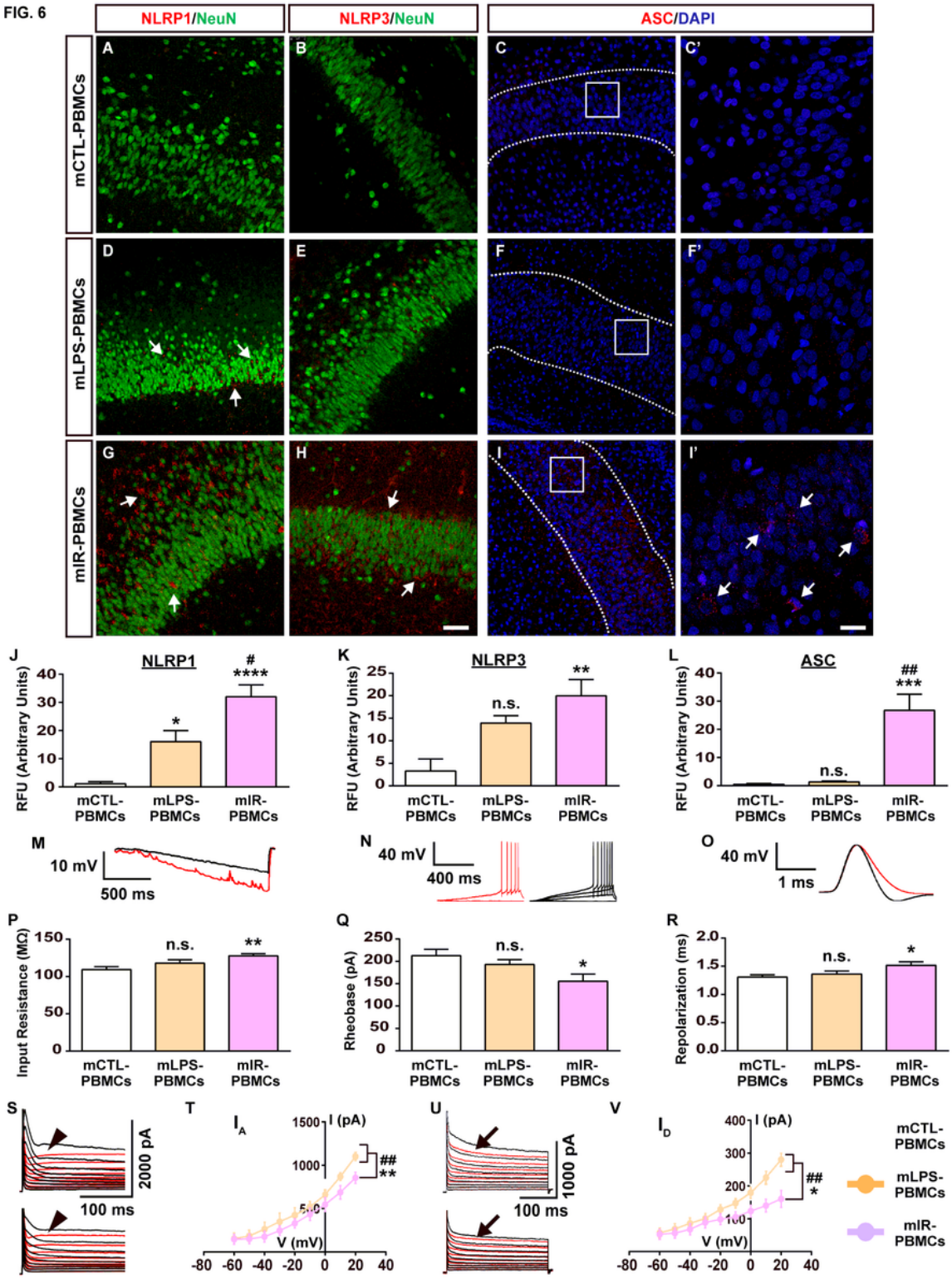

Figure 6

Cell-cell contact between LPS-PBMCs and OCHSCs is necessary for transduction of peripheral inflammation. (A-I´) Immunohistochemistry images of NLRP1/NeuN (A, D, G), NLRP3/NeuN (B, E, H) and ASC/DAPI (C, C´, F, F´, I, I´) in the hippocampus of mCTL-PBMC-OCHSCs (A-C´), mLPS-PBMC-OCHSCs (D-F´) and mIR-PBMC-OCHSCs (G-I´). C´, F´, I´ are magnified images of white boxes in C, F, I, respectively. White arrows in D, G, H, I´ mark inflammasome marker upregulation. (J) NLRP1, (K) NLRP3 and (L) ASC mean

semi-quantitative immunofluorescence in hippocampal tissue of mCTL-PBMC-OCHSCs (NLRP1: n = 5; NLRP3: n = 4; ASC: n = 4), mLPS-PBMC-OCHSCs (NLRP1: n = 5; NLRP3: n = 5; ASC: n = 4) and mIR-PBMC-OCHSCs (NLRP1: n = 5; NLRP3: n = 5; ASC: n = 4). (M) input resistance, (N) rheobase and (O) repolarization sample outputs from mCTL-PBMC-OCHSCs (black) and mIR-PBMC-OCHSCs (red) hippocampal neurons, using Figures 4P, 4Q, 4R input protocols, respectively. (P) input resistance, (Q) rheobase and (R) repolarization time bar graphs of mCTL-PBMC-OCHSCs (n = 11), mLPS-PBMC-OCHSCs (n = 11) and mIR-PBMC-OCHSCs (n = 10) hippocampal neurons. (S) IA and (U) ID sample outputs from mCTL-PBMC-OCHSCs (top) and mIR-PBMC-OCHSCs (bottom), using Figures 5F and 5M input protocols (black traces: baseline, red traces: +4-AP; see Figure 5 legend). Black arrowheads and black arrows respectively denote maximum IA and ID in S and U (see Figure 5 legend). (T) IA and (V) ID I-V graphs of hippocampal neurons from mCTL-PBMC-OCHSCs (light grey) (IA, n = 6; ID, n = 8), LPS-PBMC-OCHSCs (orange) (IA, n = 5; ID, n = 8) and IR-PBMC-OCHSCs (pink) (IA, n = 5; ID, n = 7). Error bars represent mean ± SEM; n.s. denotes not significant, *p < 0.05, **p < 0.01, ***p < 0.001, ****p < 0.0001 compared to mCTL-PBMC-OCHSCs; #p < 0.05, ##p < 0.01 compared to mLPS-PBMC-OCHSCs by Bonferroni test. Scale bars, 100 μm (A-I), 50 μm (C´-I´).

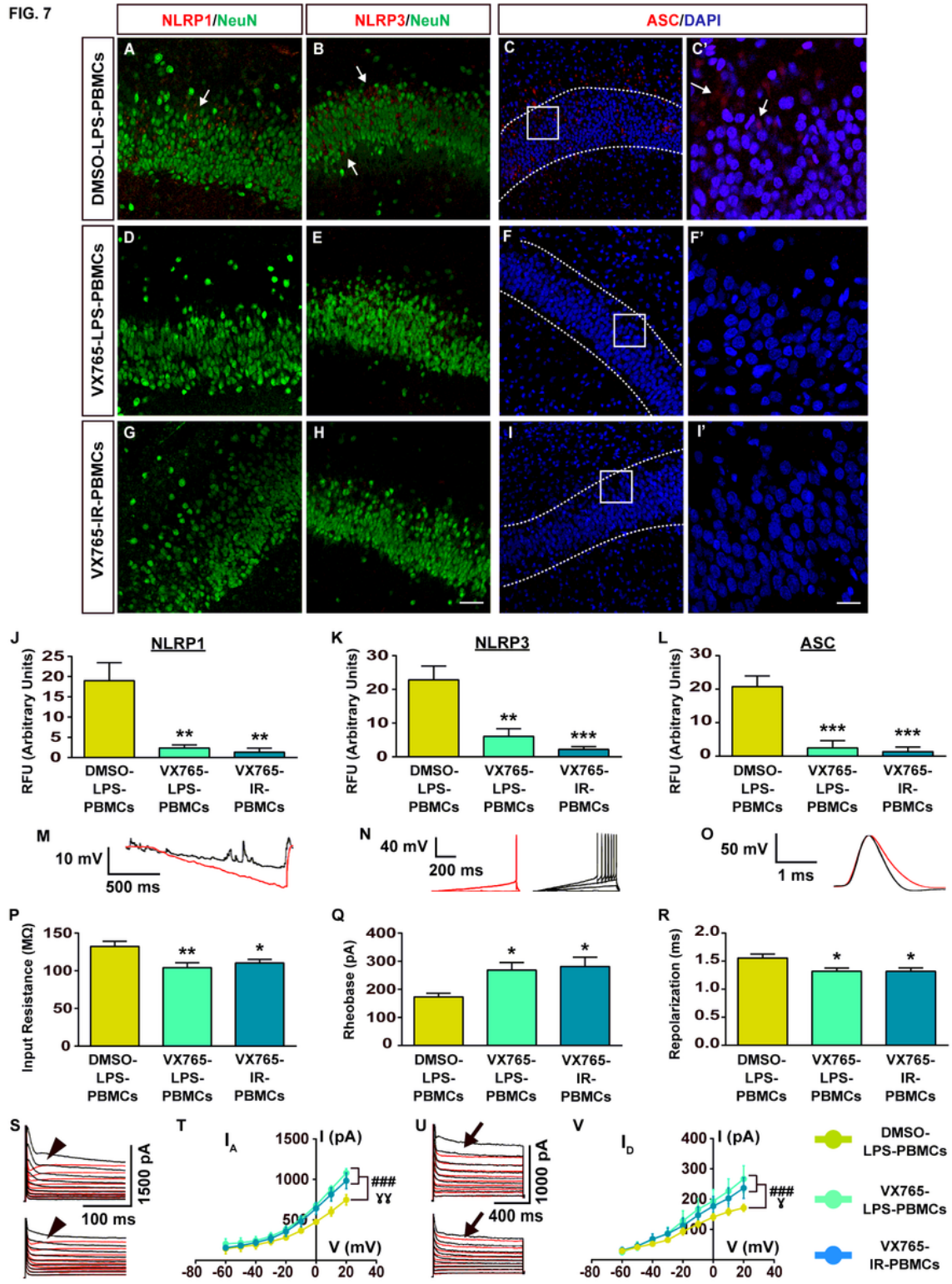

Figure 7

Inhibition of inflammasome assembly protected the hippocampus from inflammation transduction and inflammatory-coupled hyperexcitability. (A-I′) Immunohistochemistry images of NLRP1/NeuN (A, D, G), NLRP3/NeuN (B, E, H) and ASC/DAPI (C, C′, F, F′, I, I′) in the hippocampus of DMSO-LPS-PBMC-OCHSCs (A-C′), VX765-LPS-PBMC-OCHSCs (D-F′) and VX765-IR-PBMC-OCHSCs (G-I′). C′, F′, I′ are magnified images of white boxes in C, F, I, respectively. White arrows in A, B, C, C′ mark inflammasome marker

upregulation. (J) NLRP1, (K) NLRP3 and (L) ASC mean semi-quantitative immunofluorescence in hippocampal tissue of DMSO-LPS-PBMC-OCHSCs (NLRP1: n = 4; NLRP3: n = 4; ASC: n = 5), VX765-LPS-PBMC-OCHSCs (NLRP1: n = 4; NLRP3: n = 4; ASC: n = 4) and VX765-IR-PBMC-OCHSCs (NLRP1: n = 5; NLRP3: n = 5; ASC: n = 5). (M) input resistance, (N) rheobase and (O) repolarization sample outputs from VX765-IR-PBMC-OCHSCs (black) and DMSO-LPS-PBMC-OCHSCs (red) hippocampal neurons, using Figures 4P, 4Q, 4R input protocols, respectively. (P) input resistance, (Q) rheobase and (R) repolarization time bar graphs of DMSO-LPS-PBMC-OCHSCs (n = 9), VX765-LPS-PBMC-OCHSCs (n = 9) and VX765-IR-PBMC-OCHSCs (n = 9) hippocampal neurons. (S) IA and (U) ID sample outputs from VX765-IR-PBMC-OCHSCs (top) and DMSO-LPS-PBMC-OCHSCs (bottom), using Figures 5F and 5M input protocols (black traces: baseline, red traces: +4-AP; see Figure 5 legend). Black arrowheads and black arrows respectively denote maximum IA and ID in S and U (see Figure 5 legend). (T) IA and (V) ID I-V graphs of hippocampal neurons from DMSO-LPS-PBMC-OCHSCs (olive) (IA, n = 5; ID, n = 7), VX765-LPS-PBMC-OCHSCs (light blue) (IA, n = 5; ID, n = 8) and VX765-IR-PBMC-OCHSCs (navy blue) (IA, n = 5; ID, n = 8). Error bars represent mean ± SEM; *p < 0.05, **p < 0.01, ***p < 0.001 compared to DMSO-LPS-PBMC-OCHSCs; (□)p < 0.05, (□□)p < 0.01 VX765-IR-PBMC-OCHSCs compared to DMSO-LPS-PBMC-OCHSCs; (###)p < 0.001 VX765-LPS-PBMC-OCHSCs compared to DMSO-LPS-PBMC-OCHSCs; p-values calculated by Bonferroni test. Scale bars, 100 μm (A-I), 50 μm (C´-I´).

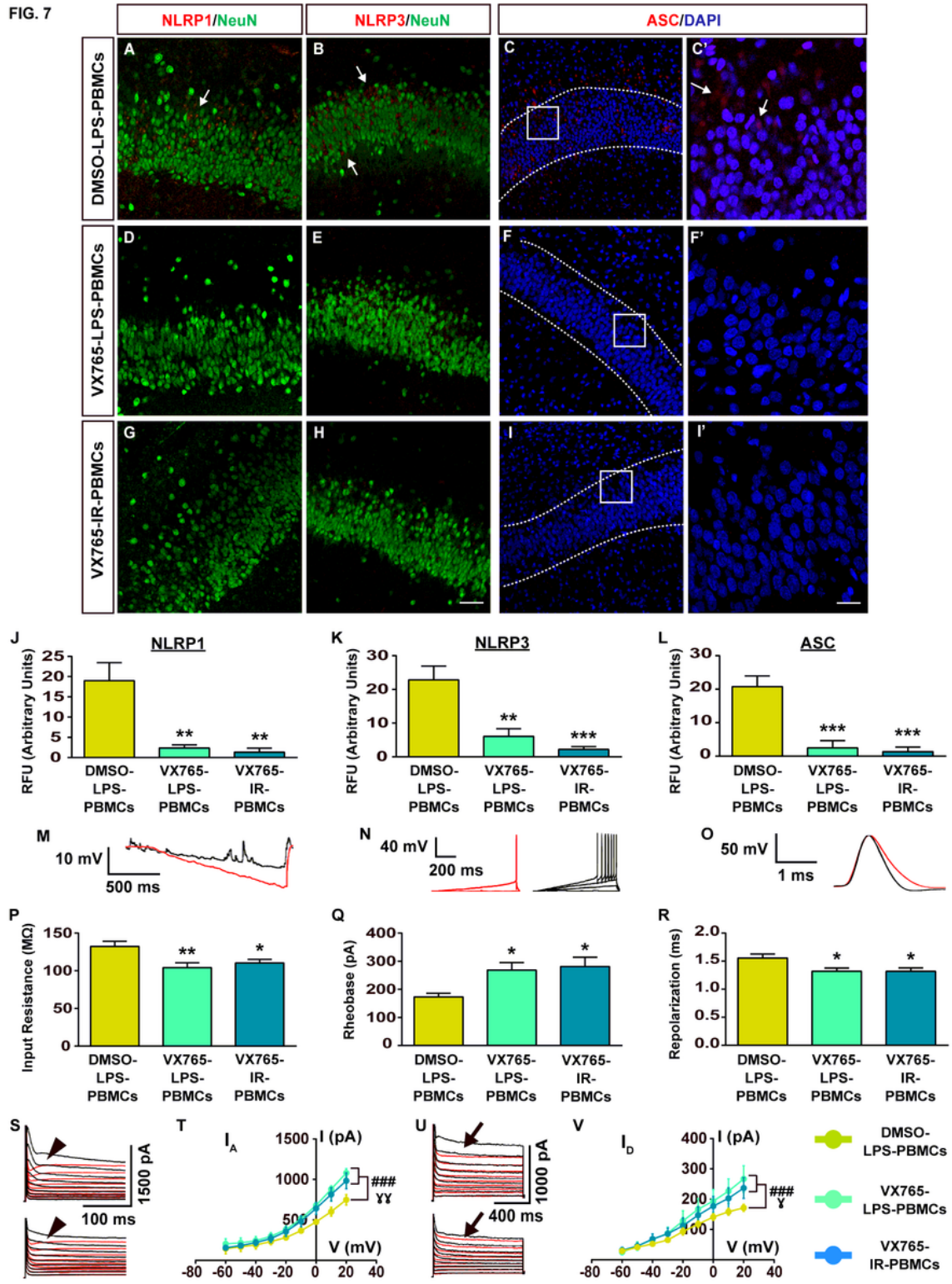

Figure 7

Inhibition of inflammasome assembly protected the hippocampus from inflammation transduction and inflammatory-coupled hyperexcitability. (A-I′) Immunohistochemistry images of NLRP1/NeuN (A, D, G), NLRP3/NeuN (B, E, H) and ASC/DAPI (C, C′, F, F′, I, I′) in the hippocampus of DMSO-LPS-PBMC-OCHSCs (A-C′), VX765-LPS-PBMC-OCHSCs (D-F′) and VX765-IR-PBMC-OCHSCs (G-I′). C′, F′, I′ are magnified images of white boxes in C, F, I, respectively. White arrows in A, B, C, C′ mark inflammasome marker

upregulation. (J) NLRP1, (K) NLRP3 and (L) ASC mean semi-quantitative immunofluorescence in hippocampal tissue of DMSO-LPS-PBMC-OCHSCs (NLRP1: n = 4; NLRP3: n = 4; ASC: n = 5), VX765-LPS-PBMC-OCHSCs (NLRP1: n = 4; NLRP3: n = 4; ASC: n = 4) and VX765-IR-PBMC-OCHSCs (NLRP1: n = 5; NLRP3: n = 5; ASC: n = 5). (M) input resistance, (N) rheobase and (O) repolarization sample outputs from VX765-IR-PBMC-OCHSCs (black) and DMSO-LPS-PBMC-OCHSCs (red) hippocampal neurons, using Figures 4P, 4Q, 4R input protocols, respectively. (P) input resistance, (Q) rheobase and (R) repolarization time bar graphs of DMSO-LPS-PBMC-OCHSCs (n = 9), VX765-LPS-PBMC-OCHSCs (n = 9) and VX765-IR-PBMC-OCHSCs (n = 9) hippocampal neurons. (S) IA and (U) ID sample outputs from VX765-IR-PBMC-OCHSCs (top) and DMSO-LPS-PBMC-OCHSCs (bottom), using Figures 5F and 5M input protocols (black traces: baseline, red traces: +4-AP; see Figure 5 legend). Black arrowheads and black arrows respectively denote maximum IA and ID in S and U (see Figure 5 legend). (T) IA and (V) ID I-V graphs of hippocampal neurons from DMSO-LPS-PBMC-OCHSCs (olive) (IA, n = 5; ID, n = 7), VX765-LPS-PBMC-OCHSCs (light blue) (IA, n = 5; ID, n = 8) and VX765-IR-PBMC-OCHSCs (navy blue) (IA, n = 5; ID, n = 8). Error bars represent mean ± SEM; *p < 0.05, **p < 0.01, ***p < 0.001 compared to DMSO-LPS-PBMC-OCHSCs; (□)p < 0.05, (□□)p < 0.01 VX765-IR-PBMC-OCHSCs compared to DMSO-LPS-PBMC-OCHSCs; (###)p < 0.001 VX765-LPS-PBMC-OCHSCs compared to DMSO-LPS-PBMC-OCHSCs; p-values calculated by Bonferroni test. Scale bars, 100 μm (A-I), 50 μm (C´-I´).

Supplementary Files

This is a list of supplementary files associated with this preprint. Click to download.

- 4AdditionalFileTableS1.docx
- 4AdditionalFileTableS1.docx
- 5AdditionalFileTableS2.docx
- 5AdditionalFileTableS2.docx